FLUORINATED RASPBERRY-LIKE PARTICLES FOR SUPERAMPHIPHOBIC COATINGS

by

Weijie Jiang

A thesis submitted to the Department of Chemistry

in conformity with the requirements for

the degree of Master of Science

Queen's University

Kingston, Ontario, Canada

(October, 2013)

Abstract

Raspberry-like polystyrene particles were fabricated through the covalent linkage of small epoxy-functionalized polystyrene particles (PS-GMA) with large amino-functionalized polystyrene particles (PS-NH_2). These covalent bonds yielded more stable and robust particle clusters than would be anticipated from non-covalent interactions. While the structures of these raspberry-like particles provided them with a dual-scale hierarchical roughness and re-entrant sites, they were further functionalized with a fluorinated random copolymer to provide them a low surface tension.

The fluorinated random copolymer used to functionalize these raspberry-like particles was poly(glycidyl methacrylate$_{20\%}$)-*co*-2(perfluorooctyl)ethyl methacrylate$_{80\%}$)$_{25}$ or P(GMA$_{20\%}$-*co*-FOEMA$_{80\%}$)$_{25}$, where the subscript 25 denotes the total number of the respective GMA and FOEMA units, while the subscript 20% and 80% denote the molar fractions of GMA and FOEMA, respectively. The epoxy groups of the GMA units could react with the amino groups of the raspberry-like particles, thus incorporating the fluorinated polymer onto the surfaces of the raspberry-like particles. In addition, the FOEMA component provided the particles with enhanced amphiphobicity.

Subsequently, these fluorinated raspberry-like particles were cast onto glass slides to demonstrate their superamphiphobic properties. These coatings exhibited superhydrophobic behavior when they were tested against water droplets. Additionally, the oil-repellency of these coatings was tested against various liquids, including diiodomethane, cooking oil, and hexadecane. The coatings exhibited superoleophobic behavior against diiodomethane and cooking oil, as well as highly oleophobic behavior against hexadecane.

This work demonstrates a simple and efficient route for the fabrication of superamphiphobic surfaces. Additionally, these surfaces are among the first examples of coatings prepared via self-assembly techniques that exhibited high repellency against hexadecane. These materials could have potential in various applications that require protection of a surface against wetting by either water or oils.

Acknowledgements

First and foremost, I would like to express my sincere gratitude to my supervisor Guojun Liu for his guidance, support and patience over the past two years. I really appreciate the opportunity that he provided for me to join his lab as a young chemist.

Furthermore, I would like to thank my fellow labmates in the Liu Group. It has been my honor and pleasure to meet and work with these fantastic people: Yu Wang, Heng Hu, Xiaoyu Li, Bolu Peng, Danielle Macoretta, Dr. Zengqian Shi, Dr. Hongbo Wang, Dr. Dean Xiong, Dr. Ian Wyman, Dr. Claudia Grozea, Dr. Muhammad Rabnawaz, Dr. John Dupont, Dr. Ganwei Zhang, and Jian Wang. Their enthusiasm, encouragement and friendship have been with me throughout the entire process. Special thanks are given to Heng Hu and Xiaoyu Li for teaching me how to use all of the lab instruments and providing me with tremendous help when I was new to the group; to Dr. Zengqian Shi for providing me with the fluorinated copolymer that has been used in this research; to John Dupont for his help with the TEM analysis; to Jian Wang for her help with the AFM and SEM analysis; to Dr. Claudia Grozea for editing my paper; and to Dr. Ian Wyman for proofreading my thesis.

Also, I would like to express my appreciation to all of my friends in Kingston. Without their friendship, I would not have such a wonderful time during the past two years. These good memories will live with me forever.

Last but not the least, I am thankful to my parents for their endless love and support along the way.

Table of Contents

List of Figures

List of Tables

List of Abbreviations

γ	surface tension
γ_{LG}	interfacial energy of the liquid/gas interface
γ_{SG}	interfacial energy of the solid/gas interface
γ_{SL}	interfacial energy of the solid/liquid interface
θ	contact angle
θ_0	intrinsic contact angle
θ_1	apparent contact angle
θ_{adv}	advancing contact angle
θ_{rec}	receding contact angle
θ_s	sliding angle
AFM	atomic force microscopy
$CDCl_3$	deuterated chloroform
cmc	critical micelle concentration
D_h	hydrodynamic diameter
DLS	dynamic light scattering
DMF	dimethylformamide
DVB	divinylbenzene
EDEA	(ethylenedioxy)bis(ethylamine)
FOEMA	2-(perfluorooctyl)ethyl methacrylate)
DRIFT-IR	diffuse-reflectance infrared Fourier-transform spectroscopy
GMA	glycidyl methacrylate
GPC	gel permeation chromatography
M_n	number average molecular weight

M_w	weight average molecular weight
NMR	nuclear magnetic resonance
PAA	polyacrylic acid
PDI	polydispersity index
P(GMA-*co*-FOEMA)	poly(glycidyl methacrylate-*co*-2(perfluorooctyl)ethyl methacrylate)
PS	polystyrene
PS-PAA	PAA-functionalized polystyrene particle
PS-GMA	epoxy-functionalized polystyrene particle
PS-NH_2	amino-functionalized polystyrene particle
PS-PVP	PVP-functionalized polystyrene particle
PTFE	polytetrafluoroethylene
PVP	poly(vinyl pyrrolidone)
R_f	roughness factor
r_l	radius of a large amino-functionalized particle
r_s	radius of a small epoxy-functionalized particle
SDS	sodium dodecyl sulfate
SEM	scanning electron microscopy
SiO_2	silica particles
St	styrene
TEM	transmission electron microscopy
TEOS	tetraethoxysilane
TFT	α, α, α-trifluorotoluene
THF	tetrahydrofuran
V50	2,2'-azobis(2-methylpropionamidine) dihydrochloride

Vinyl- SiO_2	vinyl-functionalized silica particles

Chapter 1

Introduction

1.1 Research Objectives and Organization of the Thesis

Raspberry-like particles, named after their appearance, consist of a large central particle that is surrounded by many small particles. The special dual-scale structures of these particles distinguish them as excellent candidates for enhanced surface roughness re-entrant geometries. If functionalized by low-surface-tension fluorinated moieties, films of these particles can be superamphiphobic. Thus, research of this thesis was initiated to prepare fluorinated raspberry-like polymer particles and to test their use in the fabrication of superamphiphobic surfaces. Raspberry-like polystyrene particles were fabricated by covalently linking small epoxy-functionalized polystyrene particles (PS-GMA) (Figure 1-1) with larger amino-functionalized polystyrene particles (PS-NH_2). Subsequently, these robust raspberry-like particles were reacted with the random fluorinated copolymer poly(glycidyl methacrylate-*co*-2(perfluorooctyl)ethyl methacrylate) or P(GMA-*co*-FOEMA) to yield fluorinated raspberry-like particles. Finally, the fluorinated raspberry-like particles were deposited onto glass slides to generate superamphiphobic surfaces.

This chapter describes the theoretical background of superamphiphobic coatings and the key factors that influence their performance. In addition, raspberry-like particles and their preparation techniques, as well as emulsion polymerization will be described in this chapter. The second chapter will describe the synthetic techniques for preparing the precursor particles, the raspberry-like particles, the fluorinated random copolymers, and the fluorinated raspberry-like particles. In addition, the preparation of samples and subsequent characterization via various characterization techniques, including diffuse-reflectance infrared Fourier-transform spectroscopy

(DRIFT-IR), transmission electron microscopy (TEM), atomic force microscopy (AFM), scanning electron microscopy (SEM), dynamic light scattering (DLS), and contact angle measurements will also be included in Chapter 2. Chapter 3 will focus on the Results and Discussion, including details on the morphological and topographical study of the precursor particles and the raspberry-like particles, characterization of the fluorinated random copolymers, and the superamphiphobicity of the fluorinated raspberry-like particle-based films. The summary and conclusions, as well as the proposed future work, will be presented in Chapter 4.

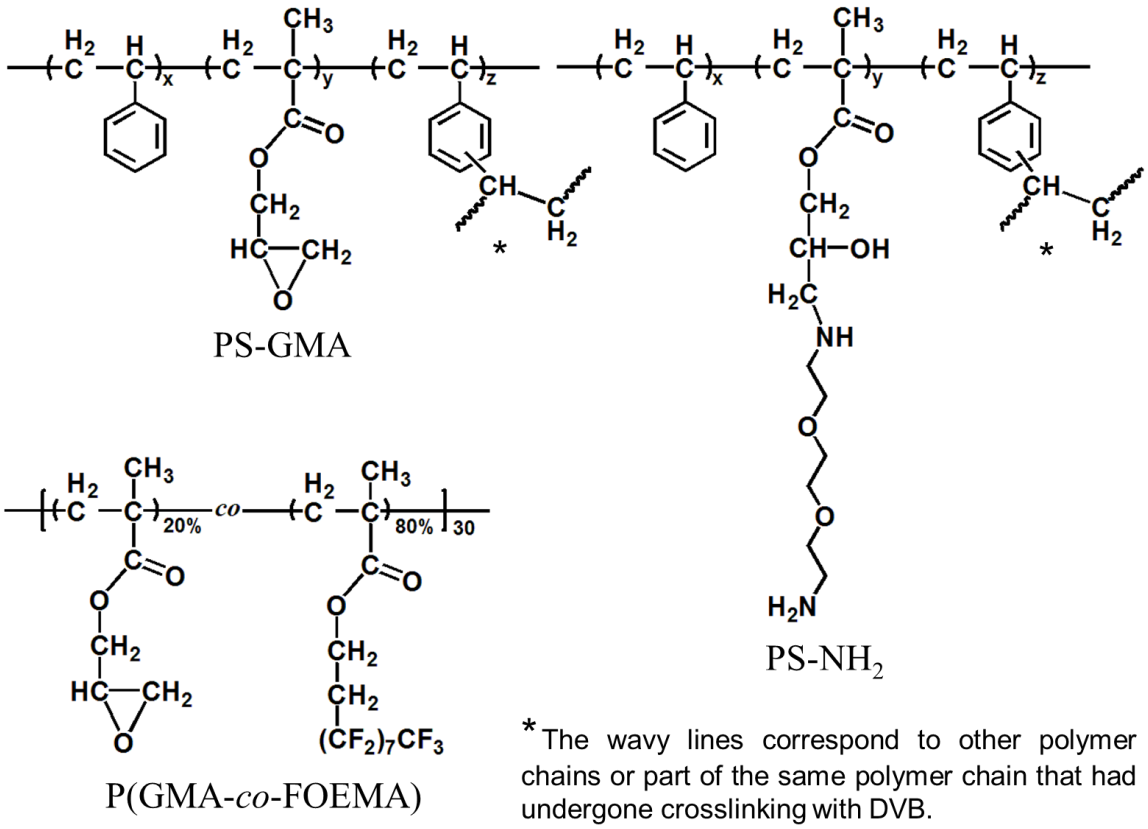

Figure 1-1 Chemical structures of PS-GMA, PS-NH2, and P(GMA-co-FOEMA).

1.2 Introduction to Superamphiphobic Surfaces

1.2.1 General Definition of Superhydrophobic Surfaces and Their Applications

A surface on which a water droplet exhibits a static contact angle of greater than 90 ° is commonly defined as a hydrophobic surface, while a surface with a static water contact angle of less than 90 ° is usually defined as a hydrophilic surface.[1] Here, the static contact angle is defined as the angle formed between the liquid/gas interface and the solid/liquid interface when a water droplet is sitting on a flat solid surface (Figure 1-2).

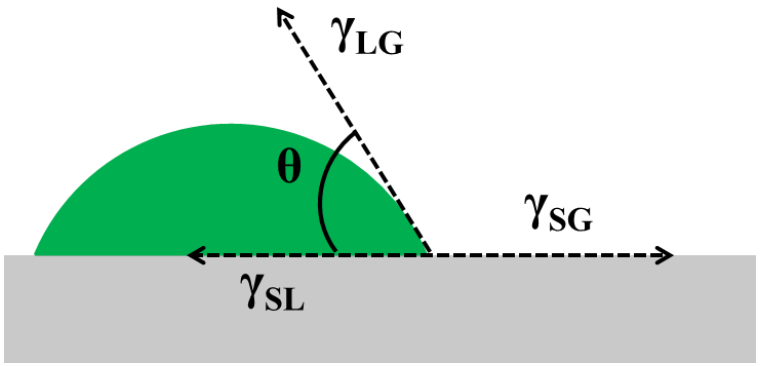

Figure 1-2 Static contact angle of a water droplet that is sitting on a flat solid surface.

However, the static contact angle along is insufficient for the characterization of the wetting or dewetting properties of a surface. In many cases, the combination of a high contact angle and a low contact angle hysteresis are considered as requirements for a self-cleaning surface.[2,3] In general, the contact angle hysteresis is defined as the difference between the advancing and the receding contact angles. As illustrated in Figure 1-3, if a small amount of liquid is added to a droplet that is sitting on a solid surface, the interfacial area of the liquid/gas interface will not change but the contact angle will increase. The maximum contact angle

achieved without changing the interfacial area is called the advancing contact angle.[2] Meanwhile, if a small amount of liquid is removed from the droplet, the interfacial area of the liquid/gas interface will remain unchanged but the contact angle will decrease. The minimum contact angle achieved without changing the interfacial area is known as the receding contact angle. If the contact angle hysteresis is sufficiently low, the droplet may roll, even if the surface is flat. However, in most cases, a droplet will not readily roll off of a flat surface unless the surface is tilted at an angle with respect to the horizontal plane. A surface with a lower contact angle hysteresis will generally require a smaller tilting angle to allow water droplets to roll. Here, the minimum angle at which a surface must be tilted to allow water droplets to roll is termed as the sliding angle, which is illustrated in Figure 1-4. The static contact angle and sliding angle are normally used to characterize the wettability of a surface.

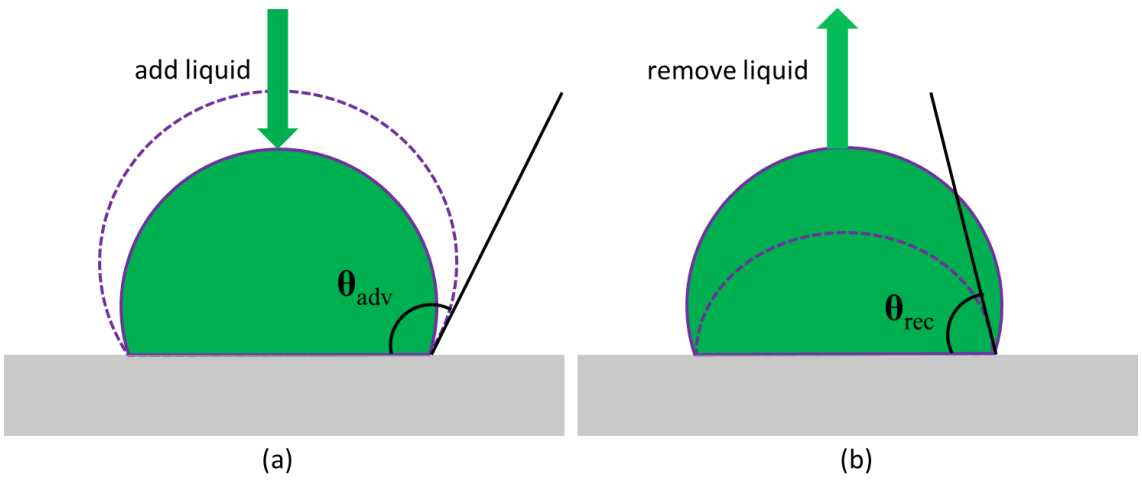

Figure 1-3 A small amount of liquid is added to or removed from a liquid droplet that is placed on a solid surface, causing the droplet to exhibit advancing (a) or receding (b) contact angles (θ_{adv} and θ_{rec}, respectively).[2]

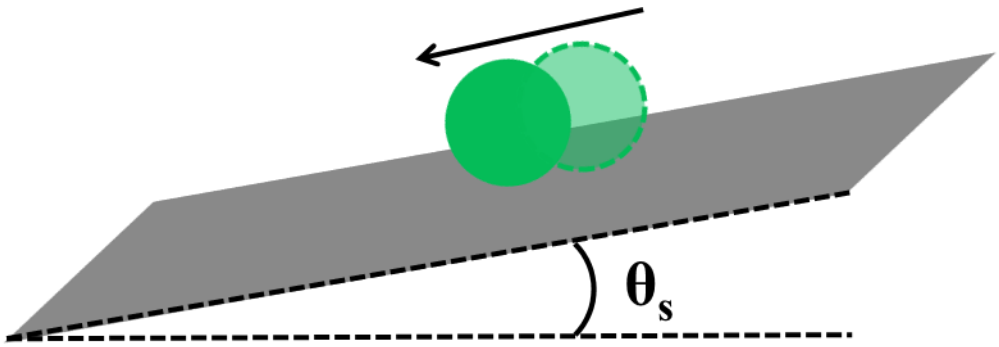

Figure 1-4 Sliding angle θ_s of a water droplet that is placed on a tilted surface.

Superhydrophobic surfaces are those on which a water droplet exhibits a static contact angle of greater than 150 ° and a sliding angle of less than 10 °.[4] These surfaces haven been widely investigated in recent decades, because of their various applications as self-cleaning, corrosion resistant, anti-fogging, and anti-icing coatings.[2-6] For example, self-cleaning windows that remain free of dirt and grime could be used in skyscrapers, largely dispensing with the need for the time-consuming and dangerous cleaning treatment. Meanwhile, ice-resistant coatings could be applied to car windshields so that no effort would be required to scrape ice off the windshields on cold winter mornings, an especially important consideration in Canada.

However, these superhydrophobic surfaces can still easily become contaminated when organic liquids such as alcohol or oil-based substances are introduced to these surfaces. Consequently, the superhydrophobicity of these surfaces becomes compromised.[7] For instance, 300 birds died after an oil spill in Alberta in 2008[8] despite the fact that their feathers were superhydrophobic. If their feathers were also superoleophobic, the oil would not have been able to wet their wings and they may have survived.

1.2.2 General Definition of Superoleophobic Surfaces and Their Applications

By analogy, a surface on which an oil droplet exhibits a static contact angle of greater than 90^{o} is commonly defined as an oleophobic surface, while a surface with a static oil contact angle of greater than $90°$ is usually defined as an oleophilic surface. When the static contact angle of an oil droplet exceeds $150°$ and the sliding angle is less than 10^{o}, the surface is described as a superoleophobic surface.[2-3] These superoleophobic surfaces have recently attracted a great deal of attention due to their various potential applications as anti-bacterial and anti-fouling coatings as well as for oil/water separations. For example, paper can be modified with coatings that impart it with excellent toner and ink repellency, thus providing an improved printing speed and printing quality.[9]

While it is beneficial for many materials to exhibit either superhydrophobicity or superoleophobicity, it is highly desirable for surfaces to exhibit both of these properties in many applications. For instance, touchscreen devices such as smartphones should be simultaneously superhydrophobic and superoleophobic, so that no water, fingerprints, or stains would remain on the screens.

1.2.3 General Definition of Superamphiphobic Surfaces and Their Applications

A surface that simultaneously exhibits superhydrophobic and superoleophobic properties is defined as a superamphiphobic surface.[2-3] Besides their significance in self-cleaning applications, superamphiphobic surfaces have also shown promising potential for the preparation of anti-reflective, corrosion resistant, anti-bacterial, and heat-resistant surfaces.[2-3] While there is an increasing demand for this unique property, achieving superamphiphobicity is often difficult.

1.3 Three Key Factors for Constructing Superamphiphobic Surfaces

Lotus leaves provide a good example of naturally-occurring superhydrophobic surface.[10] Rain droplets can pick up the dirt particles from the surface of the leaf and then roll of the surface, thus leaving behind a clean lotus leaf. Lotus leaves have inspired researchers to prepare a wide range of artificial superhydrophobic surfaces by mimicking the morphology of these leaves.[2-6] It has been proven that a low surface energy and surface roughness play complementary roles in the fabrication of superhydrophobic surfaces. However, superoleophobicity is more difficult to achieve than superhydrophobicity, because the surface tensions of organic liquids are often lower than that of water. Although there are no well-known samples of superamphiphobic surfaces observed in nature, it has been reported that a re-entrant geometry is another essential factor for providing a surface with superamphiphobicity.[11-16] Overall, a low surface energy, surface roughness and a re-entrant geometry are three key factors for the construction of a superamphiphobic surface.

1.3.1 Surface Energy

The chemical composition of a material's surface determines its surface energy, which significantly influences the contact angle of a liquid droplet that is placed on that surface. The static contact angle exhibited by a droplet on a flat surface is determined by Young's equation (Equation 1.1):[17]

$$\cos\theta_1 = \frac{\gamma_{SG}-\gamma_{SL}}{\gamma_{LG}} \qquad (1.1)$$

where θ_1 is the static contact angle, while γ_{SG}, γ_{SL} and γ_{LG} are the interfacial energies of the solid/gas, solid/liquid and liquid/gas interfaces, respectively. According to Young's equation, a material with a lower surface energy (small γ_{SG}) can exhibit a larger static contact angle or a

higher liquid repellency. Typically, compounds incorporating silicone or fluorine have low surface energies.[18-19]

Organic liquids such as cooking oil have surface tensions of ~ 30 mN/m.[20] For such an oil to achieve a contact angle greater than 90^o on a flat surface, the coating should have a surface tension that is less than 7.5 mN/m.[11-12,21] This value can be achieved by incorporating fluorine-containing molecules or polymers into these materials.[19] However, even on a flat film made of a fluorinated polymer, the respective maximum achievable contact angles are only approximately 120^o, 100^o and 80^o for water, diiodomethane, and hexadecane droplets with surface tensions of 72.1, 50.8, and 27.5 mN/m, respectively.[22] Thus, it is difficult to provide flat surfaces with superamphiphobic properties.

1.3.2 Surface Roughness

In addition to a low surface energy, a certain degree of surface roughness is required to provide a material with enhanced amphiphobicity.[23-30] A greater surface roughness increases the actual surface area of a material relative to its geometric surface area, which is the area of the 2-D projection of that rough surface. A large surface area, in combination with an inherent dislike for a liquid due to a low surface energy, reduces the spreading of the liquid, thus yielding a greater apparent contact angle. Therefore, introducing surface roughness can increase contact angles between a liquid and a flat surface if the surface is inherently repellant against that liquid with an intrinsic contact angle greater than 90°. Here, the intrinsic contact angle is the static contact angle of a liquid droplet that is placed on a flat solid surface.

Two basic theories should be considered when a liquid droplet is placed on a rough solid surface. If the liquid is forced into full contact with the surface, as depicted in Figure 1-5b, the situation is termed the "Wenzel State". This scenario state is described by Equation 1.2:[23]

$$\cos\theta_1 = R_f \cos\theta_0 \qquad (1.2)$$

where θ_1 is the apparent contact angle on a rough surface, θ_0 is the intrinsic contact angle on a flat surface, and R_f is the surface roughness factor, which is equal to the ratio of the actual surface area of a rough surface to the area of a 2-D projection of that surface. Thus, on a rough surface the apparent contact angle θ_1 is larger than its intrinsic contact angle θ_0 if θ_0 is larger than 90 °, because the surface roughness factor R_f is always greater than 1. In other words, a greater surface roughness increases the apparent contact angle. Additionally, the apparent contact angle exhibits a greater increase relative to the intrinsic contact angle as the surface roughness increases. The Wenzel theory artificially divides surfaces into two classes, repellant and affinitive, with a sharp dividing line placed at θ_0 = 90 °.[23] The apparent contact angle θ_1 is less than the intrinsic contact angle θ_0 if θ_0 is less than 90 °. In other words, surface roughness allows a liquid to spread over a surface that has an affinity for that liquid.

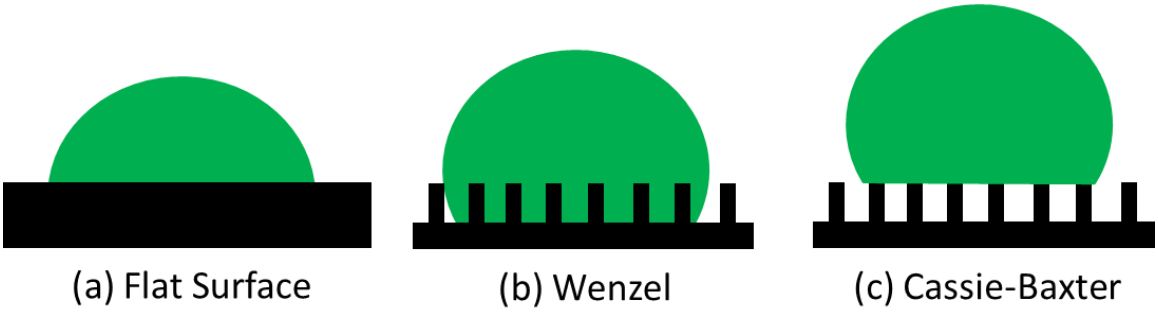

Figure 1-5 Schematic illustration of liquid droplets sitting on a flat solid surface (a) and on rough solid surfaces in the Wenzel state (b) and in the Cassie-Baxter state (c). Figure was taken out from a web source and modified.

However, the Wenzel theory has its limitations. First, the boundary (θ_0 = 90°) between an affinitive and a repellant surface is arbitrary. Second, the assumption that the droplet is in full contact with the surface is not necessarily valid if $\theta_0 > 90°$. In many cases, the liquid droplet may hang over the protrusions and trap air pockets below the droplet, as illustrated in Figure 1-5c. This situation is known as the "Cassie-Baxter state", and is described by Equation 1.3:[24]

$$\cos\theta_1 = R_f f \cos\theta_0 - (1 - f) \qquad (1.3)$$

where f and $(1 - f)$ are the fractions of the solid surface and the trapped air in contact with the liquid droplet, respectively. When f approaches 1, fewer air pockets are trapped below the droplet, and eventually the droplet becomes in full contact with the surface as f increases further to 1. Meanwhile, the apparent contact angle approaches 180° as f approaches 0 until the liquid is removed from the surface. In general, the apparent contact angle increases as f decreases. Additionally, Cassie's equation predicts that it is possible to achieve an apparent contact angle that exceeds 150°. Such a high apparent contact angle can be observed even if the intrinsic contact angle is less than 90°, provided that f is sufficiently small. For example, a θ_1 value of 150° can be calculated from Equation 1.3 by setting a θ_0 = 83°, f = 0.1, and R_f = 2.5.

In addition to a high contact angle, a low sliding angle is also necessary for applications such as self-cleaning coatings. Evidently, a droplet in the Cassie-Baxter state is more likely to roll off of a surface than one in the Wenzel state, due to the reduced contact and thus reduced van der Waals attractions between the droplet and the substrate.[23-24] In addition, the value of the apparent contact angle obtained from Equation 1.3 is typically greater than that calculated from Equation 1.2. Thus, liquid droplets are normally in the Cassie-Baxter state when they are sitting on a superamphiphobic surface.

In general, the Cassie-Baxter state is energetically more stable than the Wenzel state on intrinsically repellent rough surfaces with $\theta_0 > 90°$.[31] However, the transition from the Cassie-Baxter state to the Wenzel state is irreversible if a liquid is forced into the void spaces. This irreversibility derives from the fact that the dewetting process requires a desorption of the liquid from the solid surface and a substantial activation energy. The pressure p^* required to induce the transition from the Cassie-Baxter state to the Wenzel state is governed by the surface morphology and by θ_0.[11-12,31] Coatings with higher p^* values tend to be more robust and thus provide better candidates for demanding applications in submerged environments, such as on the hulls of ships.

However, the Cassie-Baxter state becomes less stable than the Wenzel State as θ_0 decreases below 90°. One way to stabilize this metastable Cassie-Baxter state is to create surface nano- and micro- features bearing re-entrant geometries.[11,15,31]

1.3.3 Re-Entrant Geometry

Re-entrant surfaces are those that are hidden under overhangs, and examples include the gills of a standing mushroom or the bottom half of a sphere.[11,15] The trapezoids and inverted trapezoids shown in Figure 1-6 denote the cross-sections of surface features without (a) and with (b) re-entrant sites. Since $\theta_0 < 90°$, the surface can readily undergo wetting and thus the downward movement of the liquid/air/solid tri-phase boundary can occur in both cases (a) and (b).

In case (a) shown in Figure 1-6, the downward movement of the tri-phase boundary increases f but decreases θ_1, leading to a spontaneous transition from the Cassie-Baxter state possessing a large θ_1 to the Wenzel state possessing a smaller θ_1. Meanwhile, in case (b), the downward movement of the tri-phase boundary decreases f, but increases θ_1. Consequently, the

droplets have been an even greater preference for the Cassie-Baxter state. Thus, the transition from the Cassie-Baxter state to the Wenzel state is no longer spontaneous for surfaces exhibiting re-entrant geometries. Instead, substantial activation energy is required for the transition to occur. Therefore, a re-entrant geometry can help ensure that droplets remain in the Cassie-Baxter state and thus provide a surface with superamphiphobicity, allowing it to repel low surface tension liquids such as hexadecane.

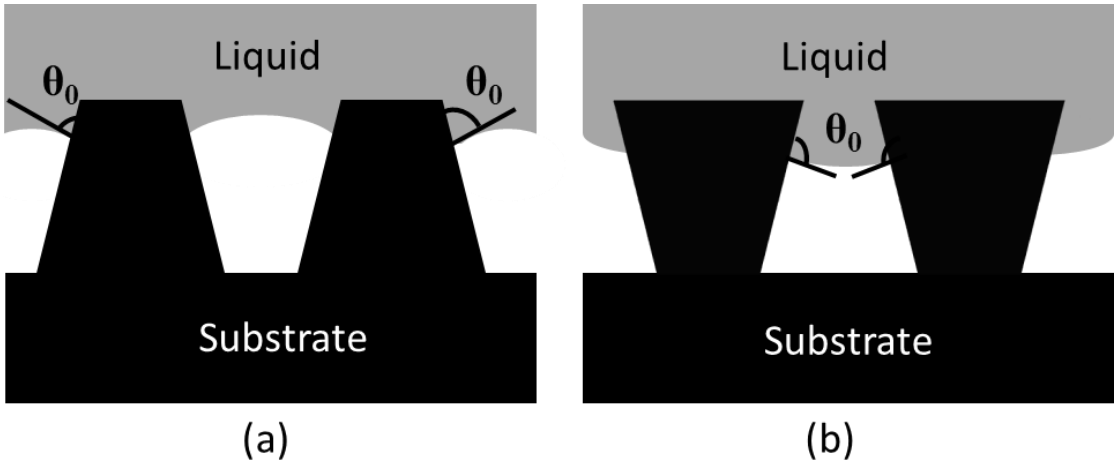

Figure 1-6 Cross-sectional diagrams of surfaces without (a) and with (b) re-entrant sites.

1.3.4 Construction of Superamphiphobic Surfaces

A low surface energy, surface roughness and a re-entrant geometry play complementary roles in providing a surface with superamphiphobicity.[16] Nano- and micro-scaled features bearing overhangs can be prepared through top-down approaches such as lithography,[32] anisotropic plasma etching,[33] electrospinning,[11-12,15] and mechanical shaping.[34] However, these approaches are expensive and difficult to perform on large scales. Bottom-up approaches involve the brushing or aero-spraying of a coating solution or dispersion onto a solid substrate and the subsequent self-assembly of the solid material into a textured coating upon solvent evaporation.[11] These methods are currently the standard protocols in use and are both economical and scalable.

However, the self-assembly of a solid material into a textured coating during solvent evaporation is challenging and demands careful design of the coating formulation.

A commonly-used method to achieve roughness and re-entrant geometries is to incorporate nanoparticles or raspberry-like particles into a coating formulation.[16,35-37] After the application of the nanoparticle dispersion onto a substrate, solvent evaporation may cause the different nanoparticles to aggregate together and stack into micrometer-sized bumps, thus providing micro-scale roughness. In addition, nano-scale roughness is obtained via the loose packing of the nanoparticles. Meanwhile, re-entrant sites occur on the bottom half of each layer of stacked nanoparticles. Coatings prepared from raspberry-like particles are especially well-suited for providing both roughness and re-entrant sites. Raspberry-like particles are formed through the fusion of small nanoparticles around a large central particle. Consequently, these particles can thus exhibit roughness on the size scales of the small and large subparticles, and the raspberry-like particles themselves.[38-40] To ensure amphiphobicity, the surfaces of these particles should be fluorinated. This can be accomplished with the use of pre-fluorinated particles or through the fluorination of these particles after they are sprayed onto the substrate. Since a thin layer of the fluorinated polymer is required to render a low surface tension to the particles, this approach uses only a small amount of the fluorinated material and is thus both practical and economical. Moreover, coatings based on fluorinated raspberry-like particles normally exhibit greater liquid repellency than those made of simple fluorinated nano- or micro-scaled particles because the former coatings have greater surface roughness.

In this work, raspberry-like polystyrene particles were modified with a fluorinated copolymer to construct superamphiphobic surfaces. Static contact angle, sliding angle, and shedding angle measurements were used to characterize the wettabilities of the fluorinated raspberry-like particle-based films. In addition, the effectiveness of the fluorinated raspberry-like

particle-based films were compared with that of films composed purely of the fluorinated copolymer, and that of films composed of fluorinated small particles.

1.4 Introduction and Preparation of Raspberry-Like Particles

Raspberry-like particles consist of a large central particle whose surface has been modified with numerous small particles, resulting in a particle cluster resembling a raspberry in shape.[38] These hierarchical structures have a dual-scale surface roughness on both nano- and micro-scale that is an important property for providing amphiphobicity. Many studies have focused on the preparation of raspberry-like particles through various simple and convenient processes.[38,40-41] Minami et al.[41] prepared raspberry-like polystyrene particles using large poly(acrylic acid) (PAA) functionalized polystyrene particles as the core and small poly(vinyl pyrrolidone) (PVP) functionalized polystyrene particles as the outer particles. These particles were synthesized via dispersion polymerization and subsequently mixed together. Raspberry-like particles were formed by hydrogen bonding interactions. Qian et al.[40] fabricated raspberry-like polystyrene/SiO_2 composite particles. First, PAA-functionalized polystyrene particles were prepared via surfactant-free emulsion polymerization. Afterwards, these particles were introduced into the hydrolysis reaction of tetraethoxysilane (TEOS) to obtain raspberry-like particles that incorporated numerous silica particles that had become adsorbed by the PAA chains attached to the central polystyrene particle. However, the resultant raspberry-like particles were not stable as the attachment of the small and large particle components relied on non-covalent interactions, rather than covalent bonds. Ming et al.[38] prepared silica-based raspberry-like particles by utilizing reactions between amino- and epoxy-functionalized silica particles. These functional silica particles were synthesized through the Stöber method and subsequently reacted together to produce covalently linked raspberry-like particles. This process required long

reaction times and many purification steps. In addition, small amino-functionalized silica particles were still present in the system after purification.

In this work, small epoxy-functionalized polystyrene particles (PS-GMA) have been prepared by emulsion copolymerization using styrene (St) as the monomer, glycidyl methacrylate (GMA) as the comonomer, divinylbenzene (DVB) as the crosslinker, and 2,2'-azobis(2-methylpropionamidine) dihydrochloride (V50) as the initiator (Figure 1-7) in the absence of a surfactant. Polystyrene (PS) seed particles have been also prepared by surfactant-free emulsion using St, DVB, and V50. Meanwhile, large PS-GMA particles were produced by seeded emulsion polymerization using St, GMA, DVB, and PS seed particles as the precursors. Subsequently, the large PS-GMA particles were converted into large PS-NH_2 particles via reaction with an excess of (ethylenedioxy)bis(ethylamine) (EDEA). Raspberry-like polystyrene particles were then fabricated by covalently linking together the small PS-GMA particles with and the large PS-NH_2 particles. Finally, these robust raspberry-like particles were functionalized with the random fluorinated copolymer poly(glycidyl methacrylate-*co*-2(perfluorooctyl)ethyl methacrylate) (P(GMA-*r*-FOEMA)) to provide these particles with a low surface tension and thus enhance their superamphiphobic properties.

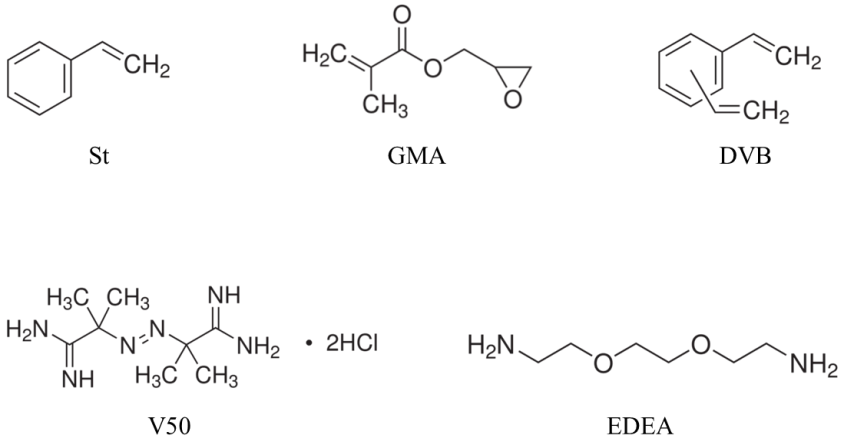

Figure 1-7 Chemical structures of St, GMA, DVB, V50, and EDEA.

1.5 Emulsion Polymerization

1.5.1 General Introduction

Emulsion polymerization is a type of free radical polymerization technique and it is one of the most common methods for polymer synthesis.[42] Polymers produced via emulsion polymerization can be used for a wide variety of applications including, but not limited to, synthetic rubbers, plastics, adhesives, and latex paints.[43-46] The environment-friendly characteristics of emulsion polymerization process have drawn significant attention, since water is used as the solvent, rather than organic solvents. In general, there are four key components required for emulsion polymerization: a water-insoluble monomer, a water-soluble initiator, a surfactant, and water.[42] An emulsion polymerization process usually begins with an oil-in-water emulsion, in which the monomer droplets are emulsified with surfactants in an aqueous phase with the aid of mechanical stirring. The polymerization is then initiated by free radicals that are generated by the initiator.

1.5.2 Ingredients for a Conventional Emulsion Polymerization

As mentioned above, four ingredients of an emulsion polymerization reaction include a monomer, an initiator, a surfactant, and water which serves as the reaction medium. These components, as well as crosslinkers, are described briefly in the following paragraphs.

Monomers. Suitable monomers for emulsion polymerization are usually insoluble or poorly soluble in water and are capable of undergoing free radical-initiated polymerization. Examples of such monomers include styrene and methyl methacrylate.[47-48] High monomer solubility may yield a polymer that is also soluble in water, instead of an insoluble polymer that aggregates to form the desired particles.[49] A co-monomer is often used in the emulsion

polymerization in order to modify the properties of the resulting polymer particles, such as the solubility, the glass transition temperature, or the mechanical properties.[50-52] For example, the copolymerization of styrene with a small amount of acrylic acid can improve the stability of the resultant polystyrene dispersion, since acrylic acid provides better solubility in water.

Initiators. Two different types of initiation methods are commonly used to generate free radicals to induce emulsion polymerization, namely thermal initiation and redox initiation. Persulfate salts and azo compounds are typically used in thermal initiation.[53-55] When they are heated in an aqueous solution, both a persulfate ion and an azo compound can generate free radicals. The mechanism for the thermal decomposition of potassium persulfate[54] and 2,2'-azobis(2-methylpropionamidine)dihydrochloride (V50)[55] are shown in Figures 1-8 and 1-9, respectively. Persulfate salts, in combination with a reducing agent such as sodium bisulfate, are usually used for redox initiation.[53] The redox reaction between a persulfate ion and a bisulfite ion is shown in Figure 1-10. Both thermal and redox initiation are widely used techniques. Redox initiation is also compatible with thermally sensitive materials, since it can be performed at low temperatures.

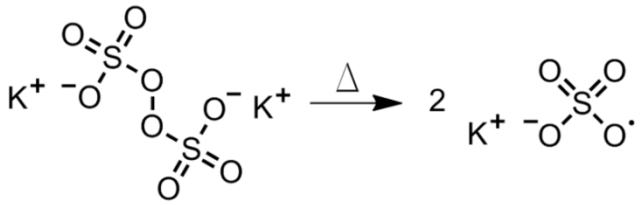

Figure 1-8 The thermal degradation of potassium persulfate.

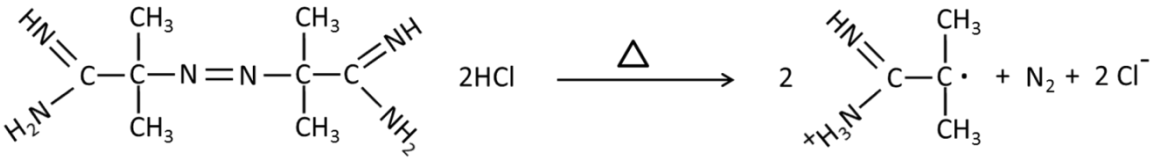

Figure 1-9 The thermal decomposition of V50.

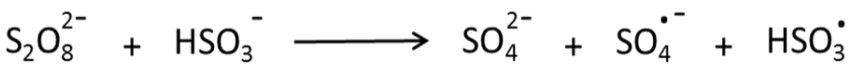

Figure 1-10 The redox reaction between a persulfate ion and a bisulfite ion.

Surfactants. Surfactants are amphiphilic molecules, containing both a hydrophilic (water-loving) "head" group and a hydrophobic (water-hating) hydrocarbon-based "tail". Generally, surfactants can be grouped into four different categories according to the composition of their polar head groups. These categories include anionic, cationic, zwitterionic, and non-ionic surfactants.[56] As shown in Figure 1-11, an anionic surfactant such as sodium dodecyl sulfate (SDS) has a negatively charged polar head group. Meanwhile, a cationic surfactant such as cetrimonium bromide has a positively charged polar head group. If a surfactant possesses a head group that bears both a negative and a positive charge, it is known as zwitterionic surfactant such as cocamidopropyl betaine. Meanwhile, a non-ionic surfactant does not have any charge on its polar end, and an example of such a surfactant includes glycerol monolaurate.

When a surfactant is dispersed into an aqueous solution, above a certain concentration called the critical micelle concentration (cmc), the surfactant monomers aggregate to form micelles (Figure 1-12). These micelles consist of a hydrocarbon-based core that is surrounded by a shell of polar head groups that are exposed to the surrounding water. Meanwhile, the micellar cores can solubilize "oily" materials and thus stabilize them in aqueous solutions.[57-58] Therefore, a surfactant not only stabilizes the monomer droplets in the aqueous phase, but can also stabilize the particles that are formed via emulsion polymerization. Additionally, the selection of an appropriate surfactant is a crucial consideration, since surfactant molecules will become incorporated into the resultant particles and thus can affect their properties.[59]

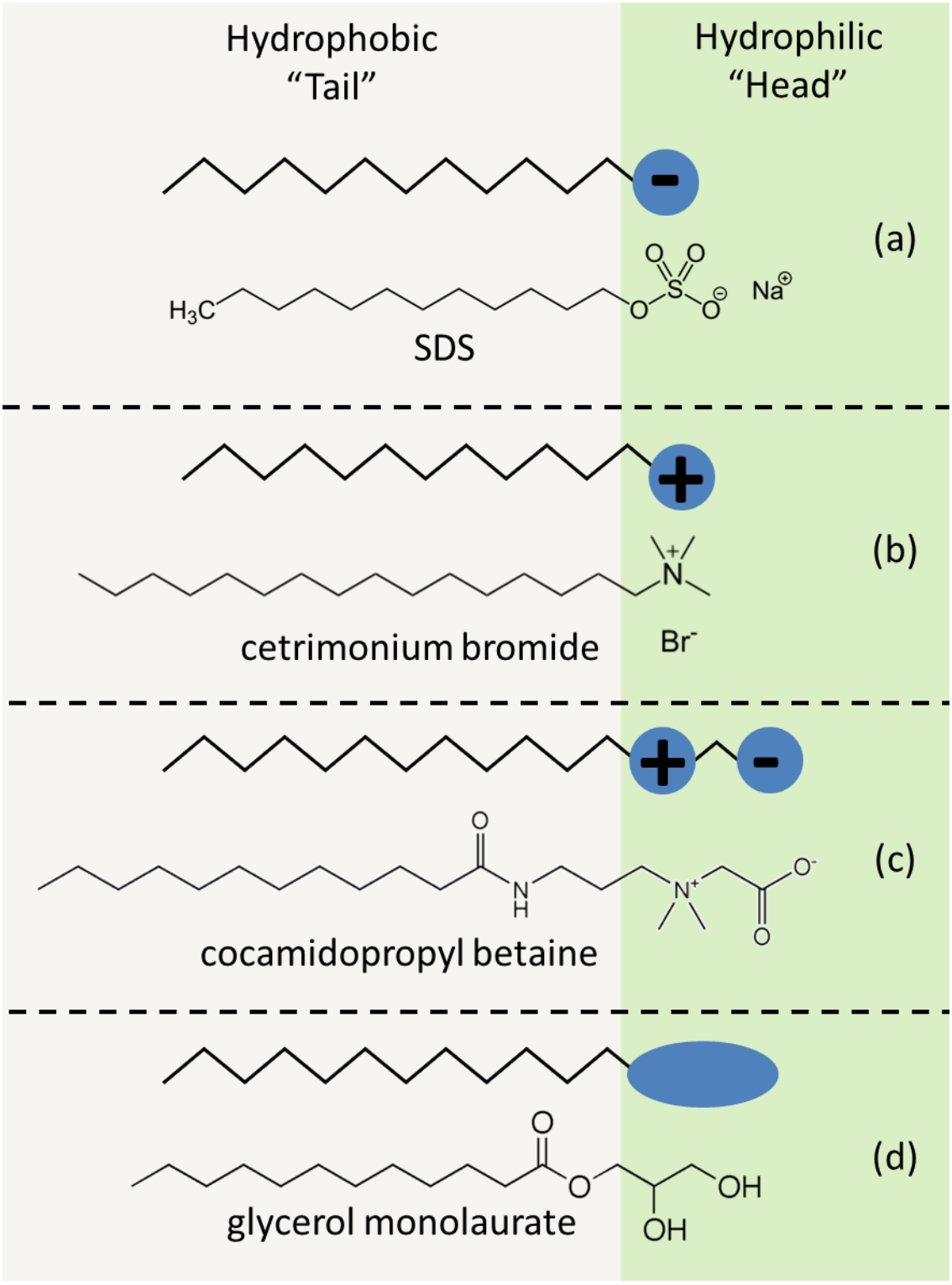

Figure 1-11 Four different types of surfactants, including anionic (a), cationic (b), zwitterionic (c), and non-ionic (d) surfactants. Examples are also shown for each type of surfactant. Figure was taken out from a web source and modified.

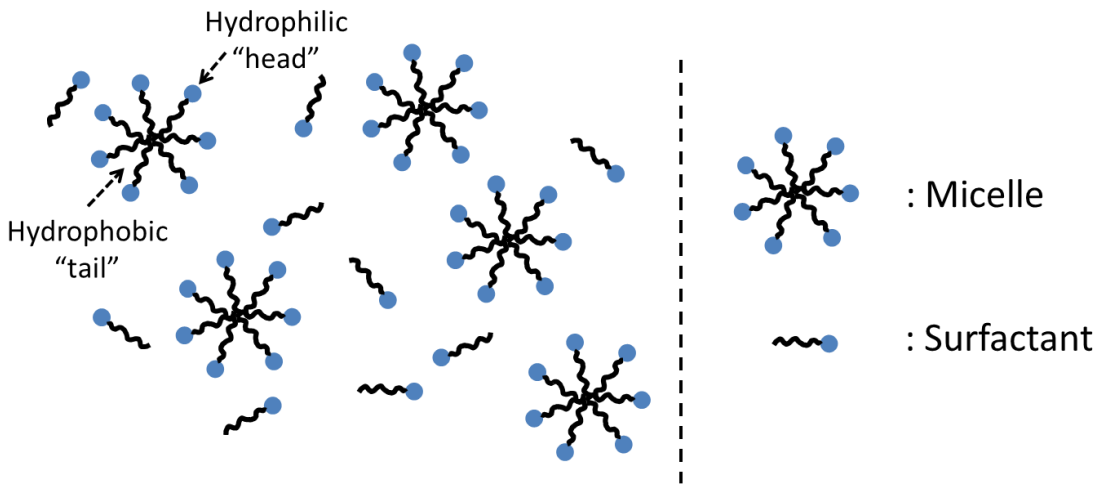

Figure 1-12 The formation of surfactant-based micelles in the aqueous phase. Micelles are formed when the surfactant is at a concentration above its cmc.

Crosslinkers. Crosslinkers or crosslinking agents are often used to link different polymer chains together during the polymerization process.[60] When polymer chains are crosslinked, they become less mobile, and the extent to which their mobility is diminished depends on the crosslinking density. An appropriate crosslinking density can ensure that the resultant particles have a rigid morphology, so that they will not deform or dissociate in a good solvent that would otherwise solubilize the individual polymer chains. Consequently, the particles are sufficiently robust so that they can be modified further.

1.5.3 Mechanism of a Conventional Emulsion Polymerization

The mechanism of a conventional emulsion polymerization normally involves three stages, depending on the particle formation process involved.[61-62] At the beginning of the first stage, the surfactants are initially dissolved in water at a concentration above their CMC, so that they form micelles. In an aqueous surfactant solution, the monomer is added and forms relatively

large droplets. A small fraction of the monomer diffuses into the micellar cores from the aqueous phase due to osmotic forces. The micelles that incorporate the monomer within their cores are defined as monomer-swollen micelles.[61]

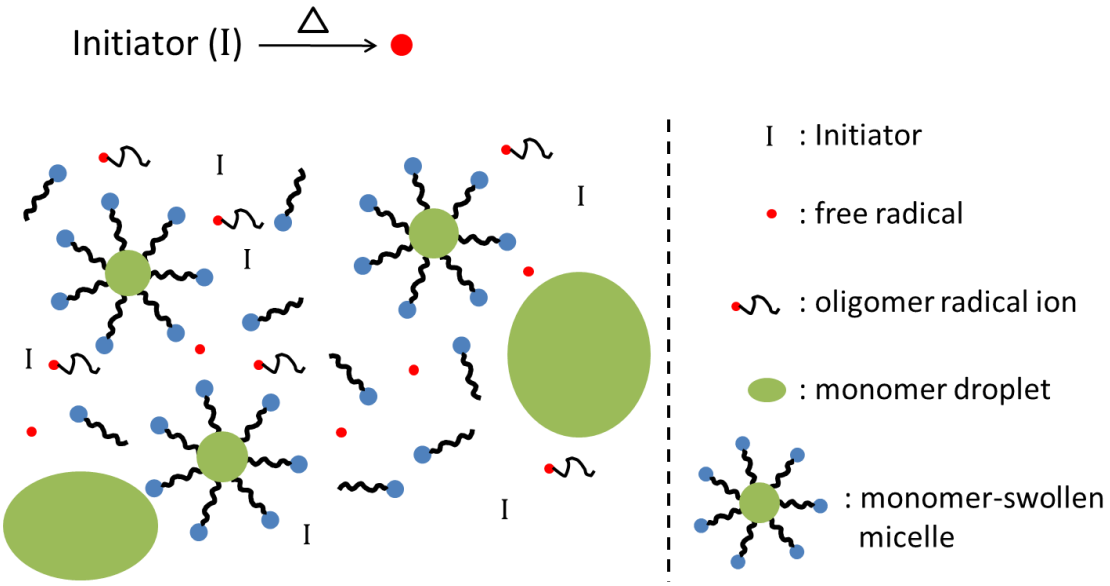

Figure 1-13 Schematic diagram depicting the beginning of the first stage of a conventional emulsion polymerization. The initiators decompose at high temperature, generating free radicals. These free radicals subsequently react with the monomer in the aqueous phase, forming short chain oligomer radical ions.

At the beginning of the first stage of a conventional emulsion polymerization depicted in Figure 1-13, a water-soluble initiator is introduced into the system and decomposes at a high temperature, thus generating water-soluble free radicals. These water-soluble free radicals quickly react with water-insoluble monomers that are dispersed in the aqueous phase. The products of these reactions contain charged ions at one end and hydrocarbon radicals at the other end, and are thus known as oligomer radical ions.[61] As these oligomer radical ions react further with more monomers, their hydrocarbon chains grow longer and they become more hydrophobic. When the oligomer radical ions become insoluble in water, they migrate into the micelles and

initiate polymerization within the micelles. At this point, the monomer-swollen micelles have been become converted into polymer particles. In order to stabilize the growing particles, more surfactants are adsorbed onto the particles. When no more surfactant is available to generate new particles, as depicted in Figure 1-14, the number of particles remains constant and the first stage of polymerization is complete.

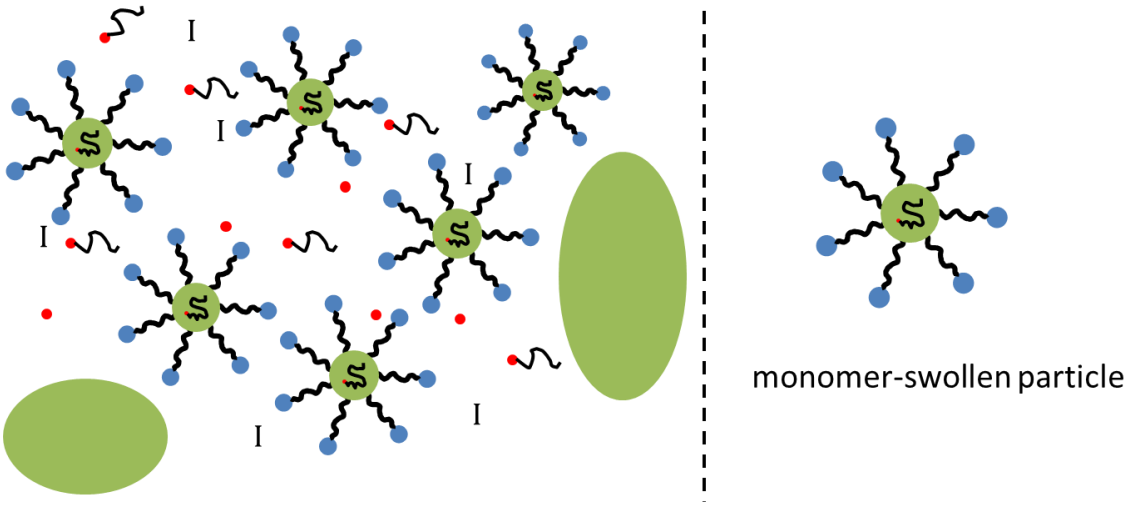

Figure 1-14 Schematic depiction of the end of the first stage of a conventional emulsion polymerization. At this point all of the free surfactants and micelles have been consumed. The free surfactants have been adsorbed onto the particles, while the micelles have been converted into monomer-swollen particles. The number of particles remains constant.

During the second stage of an emulsion polymerization, the diffusion rate is much faster than the polymerization rate. Consequently, more of the monomer diffuses from the monomer droplets to the growing particles and undergoes polymerization, while the concentration of the monomer inside the particles remains constant. This stage is completed once all of the monomer droplets in the aqueous phase are consumed. At the third stage, the monomer inside the particles undergoes polymerization until all of the monomer is depleted.

1.5.4 Surfactant-Free Emulsion Polymerization

Many studies have been undertaken to synthesize polymers via surfactant-free emulsion polymerization, since it is very difficult to remove surfactants that have become adsorbed onto the resultant polymer particles. The mechanism of a surfactant-free emulsion polymerization is very similar to that of an ordinary emulsion polymerization, except that surfactants are not involved.[63-65] The mechanism of a surfactant-free emulsion polymerization usually involves two stages based on the locus of the main reaction. An emulsion polymerization that has been initiated by a cationic initiator in the absence of surfactant is described below with an example of this process. Additionally, the mechanism of a surfactant-free emulsion polymerization is illustrated in Figure 1-15.

At the beginning of the first stage, a cationic initiator decomposes at a high temperature to generate water-soluble free radical ions. These free radical ions react with the monomer in the aqueous phase, thus forming oligomer radical ions that consist of radicals at one end and a positive charge at the other end. As the length of the oligomer chains grow, the solubility of the oligomer radical ions decrease and they eventually become insoluble in water. These oligomer radical ions behave as surfactants and aggregate together to form "micelles." During the second stage, a small fraction of the monomers from the monomer droplets migrate into the insoluble cores of these "micelles" and undergo polymerization. At this point, monomer-swollen particles are formed and the locus of the main reaction has become transferred from the aqueous phase to the particle interior. Monomers and short chain oligomer radical ions continuously diffuse into the growing particles and undergo polymerization until all of the monomer is consumed.

Surfactant-free emulsion polymerization played an important role in the research described in this thesis. In particular, surfactant-free emulsion polymerization was used to prepare the small epoxy-functionalized particles, as well as the polystyrene seed particles.

Subsequently, seeded emulsion polymerization was used to produce larger epoxy-functionalized particles.

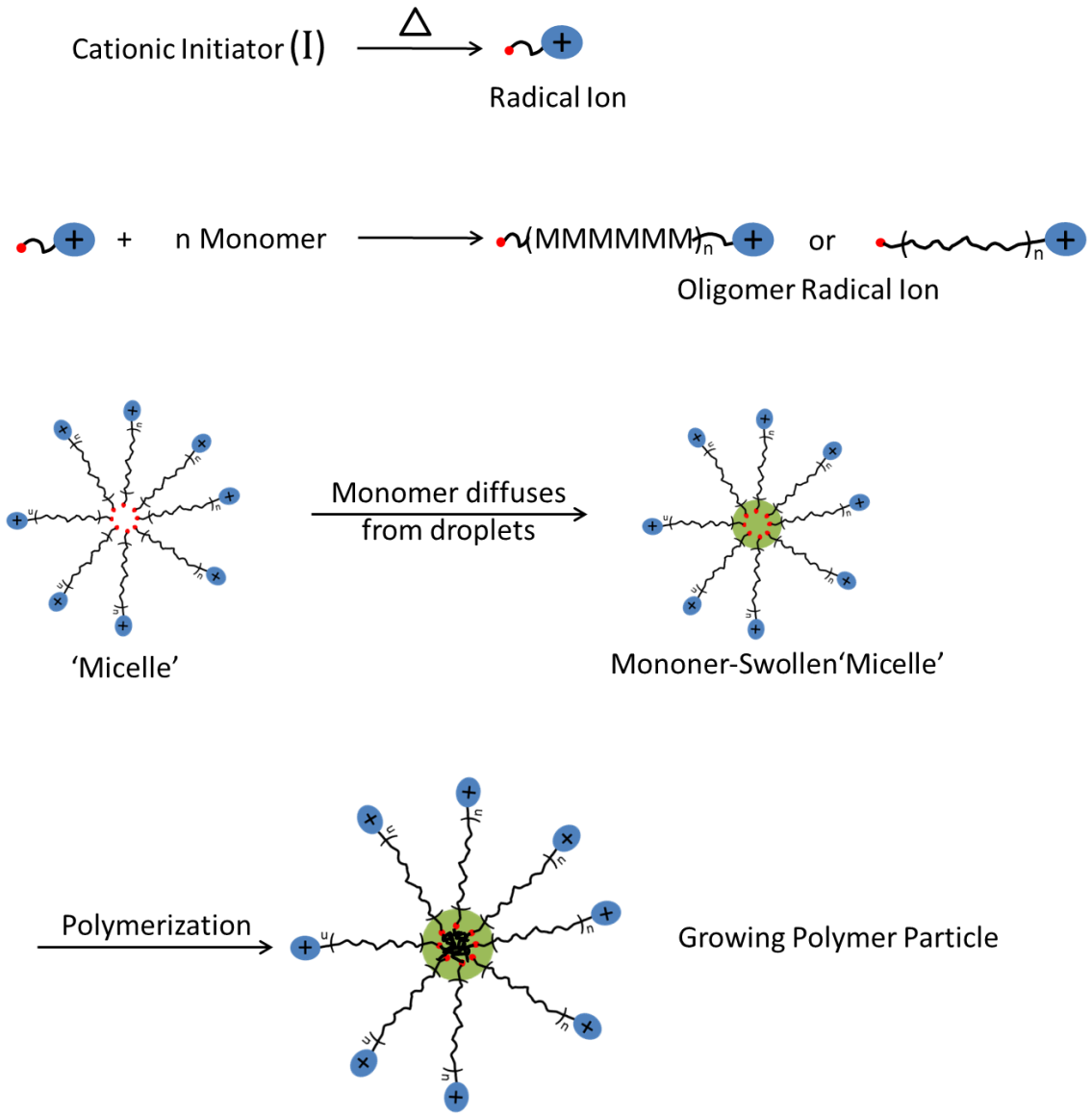

Figure 1-15 Schematic illustration of the mechanism of a surfactant-free emulsion polymerization.

1.5.5 Seeded Emulsion Polymerization

It has been demonstrated that conventional emulsion polymerization techniques can yield nano-scaled monodisperse polymer particles that range between 100 and 800 nm in diameter.[66] Multi-stage emulsion polymerization techniques involving pre-existing seed particles are usually used to produce micro-scaled polymer particles. This polymerization technique, which involves the growth of the polymer chains from the pre-existing seed particles, is often called seeded emulsion polymerization.[66] The mechanism of a seeded emulsion polymerization is also very similar to that of a conventional emulsion polymerization, except that seed particles are involved instead of surfactants.[66-68] In general, seed polymer particles are initially prepared using a surfactant-free emulsion polymerization. Subsequently, more monomer is added and reacted with the free radicals, thus yielding oligomer radical ions. As these oligomer radical ions become water-insoluble, rather than aggregating together to form new "micelles", they will become captured by the pre-existing seed polymer particles thus causing the seed particles to grow. The following reaction mechanism is similar to that of surfactant-free emulsion polymerization. The resulting particles can be used as new seed particles for preparing even larger polymer particles. Additionally, the sizes of the resulting particles increase when a large amount of the monomer is provided.

1.6 Conclusions

This chapter has provided background information on key concepts that are the basis of this thesis. In particular, the relevant information and theoretical background relating to superamphiphobic coatings and the key factors that influence their performance have been presented. Additionally, the preparation and properties of raspberry-like particles were described in this chapter. Various emulsion polymerization techniques have also been presented.

In Chapter 2, the preparation of precursor functional particles and raspberry-like particles, the synthesis of fluorinated random copolymers, and the preparation of fluorinate copolymer-functionalized raspberry-like particle-based films will be presented. In addition, characterization techniques such as DRIFT-IR, TEM, AFM, SEM, DLS, and contact angle measurements as well as the corresponding sample preparation techniques will be also included in the next chapter. Chapter 3 will focus on the Results and Discussion, including the morphological and topographical studies on the precursor particles and the raspberry-like particles, characterization of the fluorinated copolymers, and investigations on the superamphiphobicity of the fluorinated raspberry-like particle-based films. The summary and conclusions, as well as the proposed future work, will be presented in Chapter 4.

References

1. de Gennes, P. G. *Capillarity and Wetting Phenomena* **2004**.
2. Bhushan, B.; Jung, Y. C. *Prog. Mater. Sci.* **2011,** *56*, 1-108.
3. Liu, K.; Tian, Y.; Jiang, L. *Prog. Mater. Sci.* **2013,** *58*, 503-564.
4. Wang, S.; Jiang, L. *Adv. Mater.* **2007,** *19*, 3424-3424.
5. Nishimoto, S.; Bhushan, B. *RSC Adv.* **2013**, 3, 671-690.
6. Yao, X.; Song, Y.; Jiang, L. *Adv. Mater.* **2011,** *23*, 719-734.
7. McHale, G.; Shirtcliffe, N. J.; Aqil, S.; Perry, C. C.; Newton, M. I. *Phys. Rev. Lett.* **2004,** *93*, 036102.
8. Douglas, N. *Wilderness Watch* **2010,** *18*, 29.
9. Zhao, H.; Law, K.Y. *ACS Appl. Mater. Interfaces* **2012,** *4*, 4288-4295.
10. Jiang, L.; Zhao, Y.; Zhai, J., *Angew. Chem. Int. Ed.* **2004,** *43*, 4338-4341.
11. Tuteja, A.; Choi, W.; Ma, M.; Mabry, J. M.; Mazzella, S. A.; Rutledge, G. C.; McKinley, G. H.; Cohen, R. E. *Science*, **2007**, *318*, 1618-1622
12. Tuteja, A.; Choi, W.; Mabry, J. M.; McKinley, G. H.; Cohen, R. E. *Proc. Natl. Acad. Scil. USA*, **2008**, *105*, 18200-18205.
13. Zhao, H.; Law, K.Y.; Sambhy, V. *Langmuir*, **2011**, *27*, 5927-5935.
14. Zhao, H.; Park, K.C.; Law, K.Y. *Langmuir*, **2012**, *28*, 14925-14934.
15. Herminghaus, S. *Europhys. Lett.* **2000,** *52*, 165-170.
16. Deng, X.; Mammen, L.; Butt, H.-J.; Vollmer, D. *Science* **2012,** *335*, 67-70.
17. Young, T. *Philos. Trans. R. Soc. Lond.* **1805**, *95*, 65-87.
18. Mark, J. *Polymer Data Handbook*. Oxford University Press, **1999**.
19. Hirao, A.; Sugiyama, K.; Yokoyama, H. *Prog. Polym. Sci*. **2007**, *32*, 1393-1438.
20. Cao, L. L.; Jones, A. K.; Sikka, V. K.; Wu, J. Z.; Gao, D. *Langmuir* **2009,** *25*, 12444-12448.
21. Tsujii, K.; Yamamoto, T.; Onda, T.; Shibuichi, S. *Angew. Chem. Int. Ed.* **1997,** *36*, 1011-1012.
22. Campos, R.; Guenthner, A. J.; Haddad, T. S.; Mabry, J. M. *Langmuir* **2011,** *27*, 10206-10215.
23. Wenzel, R. N. *Ind. Eng. Chem*. **1936**, *28*, 988-994.
24. Cassie, A. B. D.; Baxter, S. *Trans. Faraday Soc*. **1944**, *40*, 546-551.
25. Feng, X.; Jiang, L. *Adv. Mater*. **2006**, *18*, 3063-3078.
26. Solga, A.; Cerman, Z.; Striffler, B. F.; Spaeth, M.; Barthlott, W. *Bioinspir. Biomim.* **2007,** *2*, S126-S134.
27. Nosonovsky, M.; Bhushan, B. *J. Phys. Condens. Matt.* **2008,** *20*.
28. Furstner, R.; Barthlott, W.; Neinhuis, C.; Walzel, P. *Langmuir* **2005,** *21*, 956-961.
29. Gao, X. F.; Jiang, L. *Nature* **2004,** *432*, 36-36.
30. Chen, D. Y.; Jiang, M. *Acc. Chem. Res.* **2005,** *38*, 494-502.
31. Tuteja, A. C., W.; Mabry, J.M.; McKinley, G. H.; Cohen, R. E.; Rubner, M. F. *MRS Bull.* **2008,** *33*, 752-758.
32. Im, M.; Im, H.; Lee, J. H.; Yoon, J. B.; Choi, Y. K. *Soft Matter* **2010,** *6*, 1401-1404.
33. Ellinas, K.; Tserepi, A.; Gogolides, E. *Langmuir* **2011,** *27*, 3960-3969.
34. Cui, Z.; Yin, L.; Wang, Q. J.; Ding, J. F.; Chen, Q. M. *Colloid Interf. Sci.* **2009,** *337*, 531-537.
35. Bravo, J.; Zhai, L.; Wu, Z. Z.; Cohen, R. E.; Rubner, M. F. *Langmuir* **2007,** *23*, 7293-7298.
36. Motornov, M.; Spheparovych, R.; Lupitskyy, R.; MacWilliams, E.; Minko, S. *Adv. Mater.* **2008,** *20*, 200-205.
37. Ofir, Y.; Samanta, B.; Arumgam, P.; Rotello, V. M. *Adv. Mater.* **2007,** *19*, 4075-4079.
38. Ming, W.; Wu, D.; van Benthem, R.; de With, G. *Nano Lett.* **2005,** *5*, 2298-2301.
39. Tsai, H. J.; Lee, Y. L. *Langmuir* **2007,** *23*, 12687-12692.
40. Qian, Z.; Zhang, Z. C.; Song, L. Y.; Liu, H. R. *J. Mater. Chem.* **2009,** *19*, 1297-1304.
41. Minami, H.; Mizuta, Y.; Suzuki, T. *Langmuir* **2013,** *29*, 554-560.

42. Asua, M. J. *J. Polym. Sci., Part A: Polym. Chem.* **2004,** *42*, 1025-1041.
43. Pisuttisap, A.; Hinchiranan, N.; Rempel, G. L.; Prasassarakich, P. *J. Appl. Polym. Sci.* **2013,** *129*, 94-104.
44. Li, Z.; Ma, L.; Gan, M.; Yan, J.; Hu, H.; Zeng, J.; Chen, F. *Polym. Compos.* **2013,** *34*, 740-745.
45. Gu, J.; Yan, X.; Fu, Z.; Yang, W.; Shi, Y. *J. Appl. Polym. Sci.* **2013,** *128*, 2291-2296.
46. Borthakur, J. L.; Jana, T.; Dolui, S. K. *J. Coat. Technol. Res.* **2010,** *7*, 765-772.
47. Burnett, M. G.; Lehrle, S. R. *Proc. R. Soc. Lond. A* **1959,** *253*, 331-348.
48. Sajjadi, S.; Yianneskis, M. *Polym. React. Eng.* **2003,** *11*, 715-736.
49. Kang, K.; Kan, C.; Du, Y.; Liu, D. *Eur. Polym. J.* **2005,** *41*, 439-445.
50. Lefay, C.; Charleux, B.; Save, M.; Chassenieux, C.; Guerret, O.; Magnet, S. *Polymer* **2006,** *47*, 1935-1945.
51. Mendizábal, E.; Hernández, P. J.; Puig, J. E.; Canche-Escamilla, G.; Katime, I.; Castaño, V. *J. Appl. Polym. Sci.* **1999,** *74*, 3299-3304.
52. Zosel, A.; Heckmann, W.; Ley, G.; Mächtle, W. *Colloid Polym. Sci.* **1987,** *265*, 113-125.
53. Yang, S.; Liu, H.; Zhang, Z. *Langmuir* **2008,** *24*, 10395-10401.
54. Chern, C. S. *Prog. Polym. Sci.* **2006,** *31*, 443-486.
55. Werber, J.; Wang, Y. J.; Milligan, M.; Li, X.; Ji, J. A. *J. Pharm. Sci.* **2011,** *100*, 3307-3315.
56. Schmalstieg, A.; Wasow, G. W.; Steichen, D. S.; Cox, M. F.; Floyd, D. T.; Schunicht, C.; Gruening, B. In *Handbook of Applied Surface and Colloid Chemistry*; Holmberg, K.; Shah, D.O.; Schwuger, M. J. Eds; New York, Wiley, **2002**.
57. Zana, R. *Adv. Colloid Interface Sci.* **1995,** *57*, 1-64.
58. Blandamer, M. J.; Cullis, P. M.; Soldi, L. G.; Engberts, J. B. F. N.; Kacperska, A.; Van Os, N. M.; Subha, M. C. S. *Adv. Colloid Interface Sci.* **1995,** *58*, 171-209.
59. Guyot, A.; Vidal, F. *Polym. Bull.* **1995,** *34*, 569-576.
60. Lien, S. M.; Li, W. T.; Huang, T. J. *Mater. Sci. Eng., C* **2008,** *28*, 36-43.
61. Smith, W. V.; Ewart, R. H. *J. Chem. Phys.* **1948,** *16*, 592-599.
62. van der Hoff; B. M. E. *Adv. Chem.* **1962,** *34*, 6-31.
63. Goodall, A. R.; Wilkinson, M. C.; Hearn, J. *J. Polym. Sci., Polym. Chem. Ed* **1977,** *15*, 2193-2218.
64. Ohtsuka, Y.; Kawaguchi, H.; Sugi, Y. *J. Appl. Polym. Sci.* **1981,** *26*, 1637-1647.
65. Kawaguchi, H.; Sugi, Y.; Ohtsuka, Y. *J. Appl. Polym. Sci.* **1981,** *26*, 1649-1657.
66. Eshuis, A.; Leendertse, H. J.; Thoenes, D. *Colloid Polym. Sci.* **1991,** *269*, 1086-1089.
67. Shim, S. E.; Cha, Y. J.; Byun, J. M.; Choe, S. *J. Appl. Polym. Sci.* **1999,** *71*, 2259-2269.
68. Slawinski, M.; Meuldijk, J.; van Herk, A. M.; German, A. L. *J. Appl. Polym. Sci.* **2000,** *78*, 875-885.

Chapter 2

Experimental Details

2.1 Introduction

This thesis describes the development of a simple and efficient strategy to prepare self-cleaning films that are based on fluorinated raspberry-like particles. Small epoxy-functionalized polystyrene (PS-GMA) particles, as well as polystyrene (PS) seed particles, were prepared by surfactant-free emulsion polymerization. Large PS-GMA particles were then synthesized via seeded emulsion polymerization using PS seed particles. Subsequently, large amino-functionalized polystyrene (PS-NH_2) particles were prepared by reacting the large PS-GMA particles with an excess of 2,2′-(ethylenedioxy)bis(ethylamine) (EDEA). Raspberry-like particles were prepared by covalently linking together the large PS-NH_2 particles with the small PS-GMA particles. Meanwhile, the fluorinated random copolymer poly(glycidyl methacrylate-*co*-2(perfluorooctyl)ethyl methacrylate) (P(GMA-*co*-FOEMA)) was synthesized via atom transfer radical polymerization (ATRP). After all of the exposed epoxy groups had been converted to amino groups, the raspberry-like particles were reacted with the fluorinated random copolymer P(GMA-*co*-FOEMA) to yield fluorinated raspberry-like particles. These fluorinated raspberry-like particles were subsequently deposited onto glass slides to generate superamphiphobic films.

This chapter focuses on the synthesis and characterization of the functionalized particles, the raspberry-like particles, the fluorinated random copolymer, and the superamphiphobic films. The preparation of samples for DRIFT-IR, TEM, AFM, SEM, and DLS characterization through these techniques are also described in this chapter. In addition, static contact angle, sliding angle

and shedding angle measurements that were performed to evaluate the dewetting capabilities of those fluorinated raspberry-like particle-based films are also described.

2.2 Materials

Styrene (St, 99.9%), glycidyl methacrylate (GMA, 97%) and divinylbenzene (DVB, 80%) were purchased from Aldrich and purified via distillation under reduced pressure. 2-(Perfluorooctyl)ethyl methacrylate (FOEMA, 97%) was purchased from Aldrich and purified by vacuum distillation over calcium hydride. 2,2′-Azobis(2-methylpropionamidine) dihydrochloride (V50, 97%) and 2,2′-(ethylenedioxy)bis(ethylamine) (EDEA, 98%), ethyl α-bromoisobutyrate (98%), 2,2'-dipyridine (99%), copper-(I) bromide (CuBr, 98%), *N*,*N*-dimethylformamide (DMF, 99.8%), tetrahydrofuran (THF, 99.9%), methanol (99.8%) and α,α,α-trifluorotoluene (TFT, 99%) were purchased from Aldrich and used without further purification.

2.3 Preparation of the Small and Large Epoxy-Functionalized Polystyrene Particles

The small epoxy-functionalized polystyrene (PS-GMA) particles were prepared by emulsion copolymerization[1] using styrene (St) as the monomer, glycidyl methacrylate (GMA) as the comonomer, divinylbenzene (DVB) as the crosslinker, and 2,2'-azobis(2-methylpropionamidine) dihydrochloride (V50) as the initiator in the absence of any surfactant. The recipes for preparing these particles are summarized in Table 2-1. 0.30 g of GMA and 25.0 mL of distilled water were added into a 125 mL two-neck round-bottom flask that was equipped with a mechanical stirrer. The mixture was purged of oxygen via bubbling with nitrogen gas and stirred at 300 rpm for 10 min. Subsequently, 1.00 g of St and 50.3 mg of DVB were added into the reaction flask. When the solution was heated to 90 ℃, 40.1 mg of the initiator V50 that had

been dissolved in 5.0 mL of distilled water was added to the mixture. The polymerization was continued for 3 h at 90 ℃ under nitrogen gas protection.

The large (PS-GMA) particles were prepared via seeded emulsion copolymerization[2] using PS particles as seeds as well as St, GMA, and DVB as precursors. The recipes for preparing these particles are also listed in Table 2-1. The PS seed particles were prepared first by surfactant-free emulsion polymerization. In a typical procedure, 1.00 g of St, 50.2 mg of DVB and 25.0 mL of deionized water were added into a 125 mL two-neck round-bottom flask and stirred at 300 rpm. The mixture was heated to 75 ℃ under nitrogen gas protection. Subsequently, 30.2 mg of the initiator V50 that had been dissolved in 5.0 mL of deionized water was added to the reaction flask. The reaction was allowed to proceed for 4 h. Afterwards, 1.00 g of St, 30.4 mg of GMA and 50.2 mg of DVB were also added to the reaction flask and the reaction was continued for another 12 h until the polymerization was complete.

Table 2-1 Recipes used to prepare the different-sized PS-GMA particles.

	Regent Quantities and Reaction Conditions		
Materials	Small PS-GMA Particles	PS Seeds	Large PS-GMA Particles
St (g)	1.00	1.00	1.00
GMA (g)	0.30	-	0.30
DVB (mg)	50.3	50.2	50.2
V50 (mg)	40.1	30.4	-
Water (mL)	30.0	30.0	-
Temperature (℃)	90	75	75
Reaction Time (h)	3	4	12

The resultant emulsion was filtered through an absorbent cotton sheet at room temperature to remove any precipitates. Subsequently, the PS-GMA particles were purified via three cycles involving centrifugation and re-dispersion into DMF.

2.4 Preparation of the Large Amino-Functionalized Polystyrene Particles

The large PS-GMA particles were converted into large PS-NH_2 particles via reaction with an excess of EDEA.[3] In a typical procedure, 1.50 g of EDEA was dissolved in 10.0 mL of DMF and heated to 70 ℃. Subsequently, 50 mg of the large PS-GMA particles was added drop-wise to the flask under vigorous stirring. The solution was left to react overnight. The resultant particles were purified via centrifugation and re-dispersion into DMF three times, until the supernatant obtained after the centrifugation exhibited a negative ninhydrin test.

2.5 Preparation of the Raspberry-Like Particles

The raspberry-like particles were prepared through the covalent linkage of the large PS-NH_2 particles with the small PS-GMA particles.[4] The number feed ratios of the large PS-NH_2 particles to the small PS-GMA particles used were 1:2, 1:20, 1:40, and 1:100. The raspberry-like particles prepared through these protocols will in some cases be abbreviated according to the number feed ratios that had been employed during their preparation. For example, the term 1:100 particles would represent raspberry-like particles that had been prepared using a number feed ratio of one large particle to 100 small particles. The recipes for the preparation of these raspberry-like particles are summarized in Table 2-2. A procedure based on the 1:100 number feed ratio will be described in the following sentences as an example of a typical preparation protocol. First, 25 mg of the small PS-GMA particles were dispersed into 4.0 mL of DMF and

heated to 70 ℃. Subsequently, 5 mg of the large PS-NH_2 particles were dispersed into 1.0 mL of DMF and added drop-wise into the dispersion of the small PS-GMA particles under vigorous stirring. After the addition of the solution of the large PS-NH_2 particles was complete, the mixture was left to react overnight. The resultant particles were purified via three cycles involving centrifugation and re-dispersion into DMF.

Table 2-2 Protocols used to prepare the raspberry-like particles.

	Reagent Quantities			
Materials	Ratio 1:2	Ratio 1:20	Ratio 1:40	Ratio 1:100
Large PS-NH_2 Particles (mg)	10	5	5	5
Small PS-GMA Particles (mg)	1	5	10	25
DMF (mL)	5	5	5	5

One additional reaction was performed for the protocols that were based on the 1:2 number feed ratio. First, 1 mg of the small PS-GMA particles were dispersed into 2.5 mL of DMF and heated to 70 ℃. Subsequently, 10 mg of the large PS-NH_2 particles were dispersed into 2.5 mL of DMF and quickly added to the solution of the small PS-GMA particles in a single addition under vigorous stirring. After the solution had reacted for 1 min, 0.1 mL of hexylamine was added to the reaction vial. Subsequently, the mixture was left to react overnight. The resultant particles were purified via three cycles involving centrifugation and re-dispersion into DMF.

2.6 Synthesis and Characterization of P(GMA-*co*-FOEMA)

Ethyl 2-bromoisobutyrate (26.2 mg, 134 μmol), 136.0 mg GMA (956.7 μmol) and 2.00 g FOEMA (3.76 mmol) were mixed together in a two-neck flask. Subsequently, dipyridine (63.0 mg, 403 μmol) and TFT (4.0 mL) were added to this mixture. The flask was purged with N_2 before CuBr (20.0 mg, 139 μmol) was added under a N_2 flow. The flask was degassed via three freeze-pump-thaw-N_2 refilling cycles before it was immersed into a preheated oil bath at 80 ℃. The polymerization was quenched after 2 h by immersing the reaction flask into a liquid nitrogen bath and subsequently introducing air. The crude mixture was warmed to room temperature, then passed through an alumina column using TFT as the eluent to remove ligated copper, and subsequently concentrated to 3.0 mL via rotary evaporation. This mixture was then added into 20.0 mL of methanol in order to precipitate the polymer. The precipitate was re-dissolved into 3.0 mL of TFT, and the resultant solution was added into another 20.0 mL of methanol to precipitate the polymer. This re-dissolution and precipitation procedure was repeated once again before the polymer was dried under vacuum for 24 h to yield 1.64 g of the product in a 77% yield.

Nuclear magnetic resonance (^{1}H NMR) measurements were performed with a Bruker Advance-400 instrument using a 70/30 (v/v) hexafluorobenzene/deuterated chloroform ($CDCl_3$) mixture as the solvent and a 3 s relaxation delay. The PS equivalent molecular weight M_n and the polydispersity (PDI = M_w/M_n) of the fluorinated polymer were determined via gel permeation chromatography (GPC). This GPC system was equipped with a Waters 515 HPLC pump connected to a GPC column that was packed by American Polymer Standards Corporation with 5 um AM 1000A gels. The GPC system was also equipped with a Waters 2410 refractive index detector. TFT was used as the eluent, with a flow rate of 1 mL/min at 40 ℃. Commercially available linear PS standards were used for calibration.

2.7 Preparation of Superamphiphobic Raspberry-Like Particle-Based Films

To enhance the superamphiphobicity of the target films, the raspberry-like particles were modified with the fluorinated random copolymer P(GMA-*co*-FOEMA). Before the raspberry-like particles were modified with the fluorinated copolymer, however, they were initially functionalized with amino groups. In particular, 50 mg of the raspberry-like particles were reacted with 1.50 g of EDEA to convert all of the epoxy groups on the outer surfaces of the raspberry-like particles to amino groups. To accomplish this, the EDEA was dissolved into 10.0 of mL DMF and the solution was heated to 70 ℃. This DMF dispersion of the raspberry-like particles was added drop-wise into the reaction flask under vigorous stirring before the solution was left to react overnight. The resultant particles were subsequently purified via three cycles involving centrifugation and re-dispersion into DMF, until the supernatant obtained after centrifugation exhibited a negative ninhydrin test.

Subsequently, 15 mg of the amino-functionalized raspberry-like particles described above were reacted with 50 mg of P(GMA-*co*-FOEMA) to yield fluorinated raspberry-like particles. P(GMA-*co*-FOEMA) was dissolved in 2.0 mL of TFT and the solution was heated to 70 ℃. The amino-functionalized raspberry-like particles were dispersed into a solvent mixture consisting of 0.1 and 0.9 mL of DMF and TFT, respectively, and subsequently added drop-wise into the reaction flask under vigorous stirring. After this addition, the solution was left to react overnight. The resultant particles were purified via centrifugation and re-dispersion twice into a 1:1 TFT/DMF mixture and once again into TFT. Subsequently, 15 mg of the purified particles were dispersed into 0.6 mL of TFT and this solution was then cast onto a glass plate. The solvent was then evaporated from this cast dispersion to yield the targeted film.

In addition, another glass plate was coated with the P(GMA-*co*-FOEMA) alone by casting and evaporating 0.6 mL TFT solutions containing 15 mg of the fluorinated copolymer.

Another glass plate was coated with fluorinated small particles by casting and evaporating 0.6 mL of TFT solutions containing 15 mg of the fluorinated small particles. These fluorinated small particles were prepared by reacting the small PS-NH_2 particles with P(GMA-*co*-FOEMA). To accomplish this, 50 mg of P(GMA-*co*-FOEMA) was dissolved in 2.0 mL of TFT and the solution was heated to 70 ℃. Meanwhile, 15 mg of the small PS-NH_2 particles were dispersed into a solvent mixture consisting of 0.1 and 0.9 mL DMF and TFT, respectively. Subsequently, this particle dispersion was added drop-wise to the reaction flask containing the copolymer under vigorous stirring, and the mixture was left to react overnight. The resultant particles were purified via centrifugation and re-dispersion twice into a 1:1 TFT/DMF mixture and once again in TFT.

2.8 Contact Angle Measurements

All contact angle measurements were performed at room temperature. The liquids used as the test droplets for these measurements included deionized water, diiodomethane (>99%, Aldrich), cooking oil (vegetable oil, Wal-Mart), and hexadecane (>99%, Aldrich). Various types of contact angle measurements were performed, including static contact angle, sliding angle, and shedding angle measurements.

2.8.1 Static Contact Angle Measurements

Static contact angles were measured by capturing an image of a liquid droplet using a Canon PowerShot A700 camera and processing the resulting image using the Image J software package.[5] Static contact angles were measured using 10 μL water droplets, 5 μL diiodomethane droplets, 5 μL cooking oil droplets, and 5 μL hexadecane droplets. In addition, static contact

angles were measured at ten different positions on each sample. The reported static contact angle represented the average of ten measurements.

2.8.2 Sliding Angle Measurements

Each coated glass plate was affixed to a ruler with double-sided adhesive tape.[5] As shown in Figure 2-1, one end of the ruler was placed against a horizontal metal block, while the other end was placed on the top edge of a lab jack. At the beginning of the test, both ends of the ruler were set at the same height, so that the glass plate was level. After a 10 μL droplet of an organic liquid or a 10 μL water droplet was applied onto the glass plate, the slope of the ruler was gradually increased by raising the lab jack. When the droplet began to roll, the angle θ between the slope of the elevated ruler and the horizontal plane was taken as the droplet sliding angle. For each sample, droplets were placed at five different positions on the coated glass plate. Each reported sliding angle represented the average of five measurements.

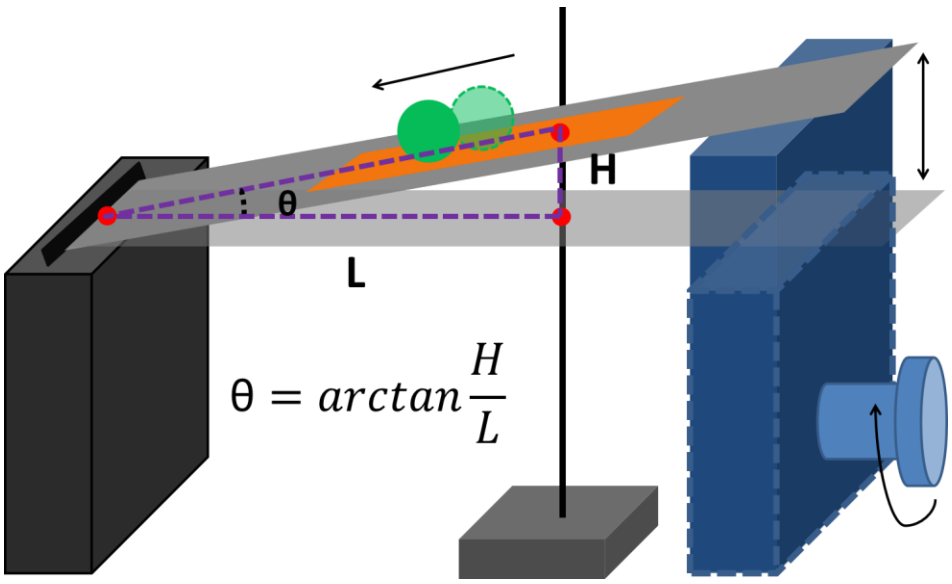

Figure 2-1 Schematic illustration of the apparatus used to perform the sliding angle measurements.

2.8.3 Shedding Angle Measurements

Each coated glass plate was attached to a ruler with double-sided adhesive tape. As depicted in Figure 2-2, one end of the ruler was placed against a horizontal metal block, while the other end was placed on the top edge of a lab jack. The tip of a low retention 0.1-10 µL adjustable pipette holding the desired test liquid was placed at a fixed distance above the coated glass plate (1 cm).[5-6] The pipette tip was positioned in a way that ensured a droplet falling from the tip would contact the coated glass plate at a position that was least 2 cm from the bottom edge. To determine the shedding angle, measurements were started at an inclination angle of 50 °. 10 µL organic liquid or water droplets were released onto the coated glass plate at five different positions. If all of the droplets rolled off the coated glass plate, the inclination angle was reduced. This procedure was repeated until one or more of the droplets would not completely roll off the surface. This inclination angle was recorded as the shedding angle.

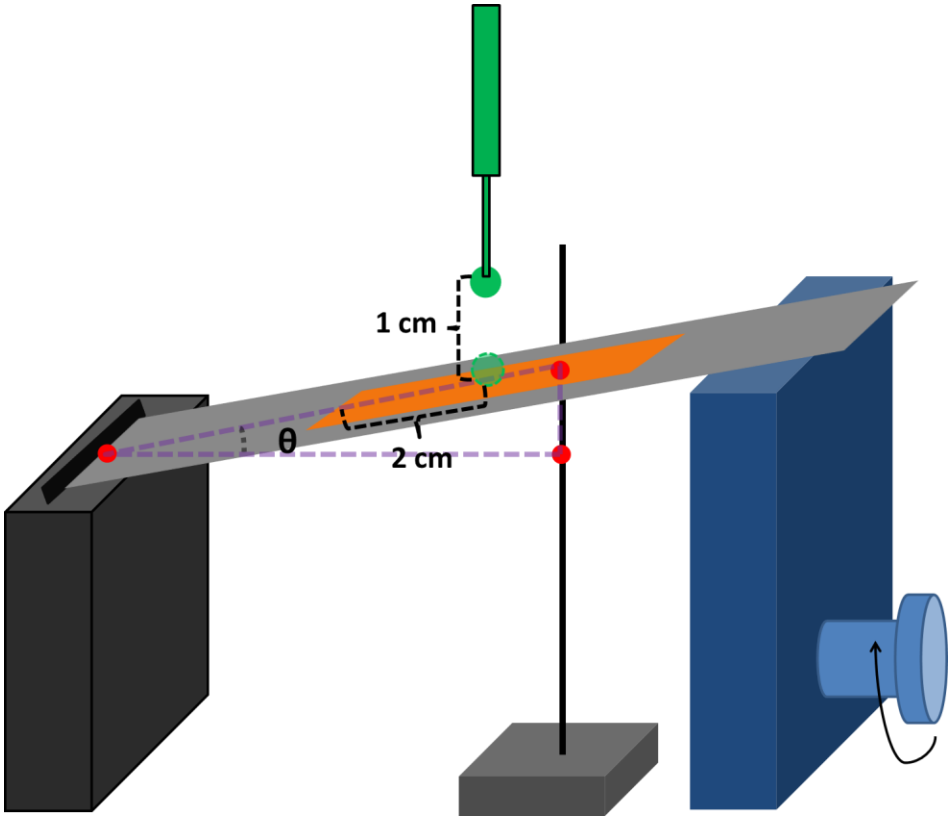

Figure 2-2 Schematic illustration of the apparatus used to perform the shedding angle measurements.

2.9 Characterization

2.9.1 Diffuse-Reflectance Infrared Fourier-Transform Spectroscopy (DRIFT-IR)

The epoxy-functionalized PS-GMA particles and the amino-functionalized particles were characterized via DRIFT-IR spectroscopy. To accomplish this, samples of the different-sized PS-GMA particles and the large PS-NH_2 were mixed with KBr and ground to yield a powder. The DRIFT-IR spectra of these samples were subsequently recorded using a Varian 640-IR FT-IR spectrometer.

2.9.2 Transition Emission Microscopy (TEM)

Samples of the different-sized epoxy-functionalized PS-GMA particles and the large amino-functionalized PS-NH_2 particles as well as various raspberry-like particles were characterized via TEM. To prepare these samples, the particles were dispersed into THF at 1 mg/mL and aero-sprayed onto carbon-coated copper grids. The samples were subsequently dried at room temperature for 2 h prior to imaging. TEM images were obtained using a Hitachi H-7000 instrument operated at 75 kV.

2.9.3 Atomic Force Microscopy (AFM)

The epoxy-functionalized PS-GMA particles, the amino-functionalized PS-NH_2 particles, and the 1:100 raspberry-like particles were also characterized via AFM. To prepare these particles for AFM characterization, they were re-dispersed into THF at 1 mg/mL and aero-sprayed onto silicon wafers. AFM images were obtained using a Veeco Multimode instrument that was equipped with a Nanoscope IIIa controller and operated in the Tapping Mode. Rectangular-shaped silicon probes (AppNano, ACT) with a 300 kHz resonance frequency and a spring constant of 40 N/m were used for the AFM characterization.

2.9.4 Scanning Electron Microscopy (SEM)

To prepare the 1:100 raspberry-like particles for SEM characterization, they were dispersed into THF at 1 mg/mL and aero-sprayed onto a silicon wafer. Meanwhile, the fluorinated small particles and the fluorinated 1:100 raspberry-like particles were cast onto glass slides. Each sample was dried at room temperature for 2 h and then coated with Au via vacuum

sputter coating. SEM images were obtained using a FEI Quanta 650 ESEM FEG MLA instrument that was operated at 10 kV.

2.9.5 Dynamic Light Scattering (DLS)

The small epoxy-functionalized PS-GMA particles, the large amino-functionalized PS-NH_2 particles and the 1:100 raspberry-like particles were dispersed into DMF at 1 mg/mL. The small epoxy-functionalized PS-GMA particles were passed through a 0.45 um PTFE (polytetrafluoroethylene) membrane filter while the large amino-functionalized PS-NH_2 particles were passed through a 1.2 um PTFE membrane filter prior to analysis. Meanwhile, the 1:100 raspberry-like particles were centrifuged at 300 rpm for 5 min before analysis. DLS measurements were performed using a Brookhaven BI-200 SM instrument that was equipped with a BI-9000AT digital correlator and a He-Ne laser. Measurements were performed at room temperature at a scattering angle of 90^{o}. The data was analyzed via the Cumulant method in order to determine the hydrodynamic diameter (D_h) and the polydispersity index (K_1^2/K_2) of the particles. The refractive index and viscosity of DMF used for these calculations were 1.4305 and 0.92 mPa·s, respectively.[7] Each reported hydrodynamic diameter and polydispersity index value represented the average of five measurements that were performed for each sample under similar conditions.

References

1. Lv, J. N.; Fang, S. J.; Chen, L., *Chinese J. of Polym. Sci.* **2009,** *27*, 101-108.
2. Shim, S. E.; Cha, Y. J.; Byun, J. M.; Choe, S., *J. of Appl. Polym. Sci.* **1999,** *71*, 2259-2269.
3. Ramos, J.; Pagani, N.; Riccard, C.; Borrajo, J.; Goyanes, S.; Mondragon, I., *Polymer* **2005,** *46*, 3323-3328.
4. Ming, W.; Wu, D.; van Benthem, R.; de With, G., *Nano Lett.* **2005,** *5*, 2298-2301.
5. Xiong, D.; Liu, G., *Langmuir* **2012,** *28*, 6911-6918.
6. Zimmermann, J.; Seeger, S.; Reifler, F. A., *Textile Research Journal* **2009,** *79*, 1565-1570.
7. Haynes, W. M. *CRC Handbook of Chemistry and Physics*. 94th ed.; CRC Press: Taylor and Francis Group: Boca Raton, FL, 2013.

Chapter 3

Results and Discussion

3.1 Introduction

Functional particles show great potential for numerous of applications ranging from drug delivery,[1-2] to sensors,[3] to photonic crystals,[4] and to electronic devices.[5] These complex particles allow the fabrication of tailored materials due to the high degree of control that is afforded to the designer during both the synthesis and assembly processes.[6-7] Particle preparation techniques include emulsion polymerization,[8-10] the use of templates,[11] lithography,[12] self-assembled heterocoagulation,[13] and various other methods. The range of functional particles fabricated has been as diverse as the number of methods used to prepare them. Some examples of this diverse range of functional particles include Janus particles[3-4,8,14-15] consisting of two unique domains with different properties, multicompartment particles based on triblock terpolymers,[16-17] as well as hierarchically structured composite particles, such as raspberry-like particles.[10-11,13,18-20]

As mentioned earlier in this thesis, raspberry-like particles are composed of a central large particle whose surface has been modified with multiple small particles, resulting in a particle cluster that resembles a raspberry in shape. These hierarchical structures have a dual-scale surface roughness which has been shown to provide superhydrophobic properties to both natural[21-22] and synthetic[23-24] materials. As mentioned earlier in Chapter 1, a surface is considered superhydrophobic if water droplets placed on that surface exhibit a water contact angle higher than 150 ° and a sliding angle of less than 10 °. However, the surface wettability is not influenced by topography alone, as the chemical composition of a material is also an important consideration. A low surface tension will enhance the hydrophobicity of the material.[21,24]

Superhydrophobic materials have great potential for many applications due to their self-cleaning properties.[21,24-25] Nevertheless, these surfaces can lose their self-cleaning capabilities when they are contaminated with oily liquids.[26] Superamphiphobic surfaces are both superhydrophobic and superoleophobic, and can thus repel both oil and water droplets. Due to this dual repellency, superamphiphobic materials are highly desirable for various practical applications.[27] Superamphiphobic materials can be used as coatings to protect metal surfaces against corrosion,[28-29] to prevent staining of fabrics,[30-32] to protect the walls of buildings against graffiti,[33-34] and for various other applications. However, superamphiphobic surfaces are more difficult to prepare than superhydrophobic surfaces due to the much lower surface tension of oily liquids as opposed to water.[27] The local surface morphology, and particularly the presence of re-entrant sites, have a key influence on the effectiveness of these materials.[35-38] Tuteja et al.[35-36] demonstrated silicon and electrospun fiber mats bearing fluorinated "microhoodoo" pillars exhibited re-entrant geometries that directly influenced the superoleophobic behavior of these surfaces, driving the systems into the superamphiphobic regime. Further studies by Zhao et al.[37-38] also confirmed these observations when they prepared fluorosilane-coated silicon pillars with various re-entrant geometries in the side walls of the pillars. In both studies, photolithography was used to pattern silica wafers with the desired geometry. Superamphiphobic materials were also obtained by coating textile fibers. Xiong et al.[32] used silica particles that were coated with a diblock copolymer incorporating a sol-gel forming block that would bind with the fibers and a fluorinated block that reduce to decrease the surface tension of the substrate. A dual-scale roughness was introduced into the system from the silica particles that became attached to the already rough textile fibers. Zhou et al.[31] employed a similar method based on silica nanoparticles to coat fibers except that they used a fluorinated polymer and a fluoroalkyl silane. A more complex method based on perfluoroalkyl silane modified silica raspberry-like particles was used by Leng et al.[39] In this case, the triple-scale roughness of the surface in conjunction

with a low surface tension drove the system into the superamphiphobic regime. Candle soot was employed by Deng et al.[40] to generate superamphiphobic glass surfaces. This was accomplished by holding a glass slide in the flame of a paraffin candle, causing the glass slide to become coated with a porous layer of soot composed of nanometer-sized carbon particles. This soot deposit was subsequently reinforced with a layer of silica and subsequently fluorinated.

In this thesis, I present a novel method to prepare superamphiphobic coatings based on fluorinated raspberry-like PS particles. This strategy involved the preparation of raspberry-like particles, using epoxy-functionalized PS particles (PS-GMA) and amino-functionalized PS particles (PS-NH_2) as precursors. A schematic illustration of the synthetic procedure used to prepare the raspberry-like particles is shown in Figure 3-1. To fabricate these raspberry-like particles, small PS-GMA particles were prepared as precursors via surfactant-free emulsion polymerization. Subsequently, large PS-GMA particles were synthesized in a similar manner using pre-made PS seeds. These large PS-GMA particles were converted into PS-NH_2 particles via a ring opening reaction with EDEA. Lastly, raspberry-like PS particles were then fabricated by covalently linking the small PS-GMA particles together with the large PS-NH_2 particles. These raspberry-like particles were then functionalized with a fluorinated random copolymer, P(GMA-*co*-FOEMA), to provide them with a low surface tension and thus enhance their superamphiphobic properties. Finally, these particles were applied onto glass substrates through a simple casting and evaporation technique to generate the superamphiphobic coatings.

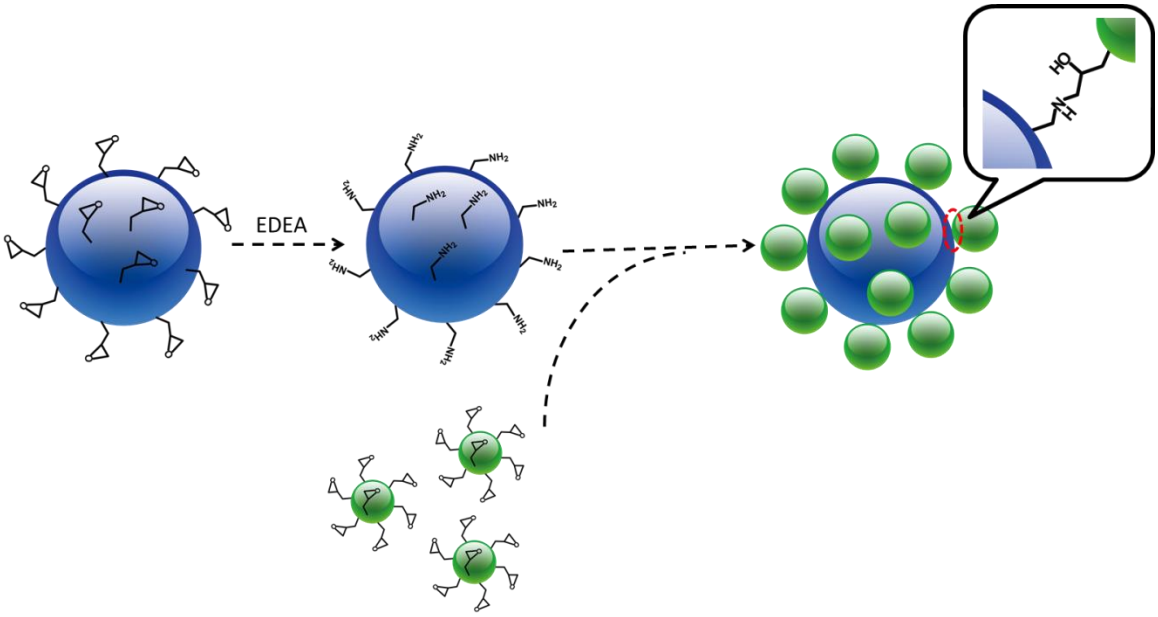

Figure 3-1 Schematic illustration of the procedure used to prepare the raspberry-like particles.

3.2 Characterization of the Precursor Functional Particles

3.2.1 Characterization of the Small Epoxy-Functionalized Polystyrene Particles

The small PS-GMA particles were prepared by the surfactant-free emulsion polymerization of styrene (St) with glycidyl methacrylate (GMA) using V50 as the initiator and DVB as the crosslinking agent. GMA was used to functionalize polystyrene particles due to its bi-functional nature. In particular, this reagent incorporated both a double bond that could bind to other polymers and an epoxy group that could undergo a ring opening reaction with amino groups.[41] V50 was used as an initiator because it not only initiated the polymerization, but also stabilized the resultant particles by providing them with positive charges.[42] Lv et al. also reported that V50 was more effective than potassium persulfate (KPS) in preventing the GMA epoxy groups from undergoing ring opening reactions during the polymerization.[43] KPS decomposed at high temperature and cause the reaction medium to become acidic, and the epoxy groups were

more readily hydrolyzed under this acidic condition. In the case of V50, the polymerization was performed under neutral conditions. In addition, DVB was used as a crosslinker to stabilize the spherical shape and monodispersity of the functional particles in subsequent reactions. Cha et al.[44] have also demonstrated previously that PS particles that had been crosslinked with DVB retained both their monodispersity and their spherical structures.

Figure 3-2a and b show the TEM image as well as the AFM images of the small PS-GMA particles. These particles were spherical and smooth, with an average TEM diameter of 120 $\pm$ 4 nm. Previous studies have shown that with a GMA content of 15-17 wt%, the particles would adopt a spherical and smooth morphology. However, as the GMA content was increased to 40-43 wt%, the particles would become rough and irregular due to an increase in the number of polar groups within the particles.[43,45-46] The small PS-GMA particles incorporating 23 wt% of GMA content, exhibited smooth and spherical structures as observed in Figure 3-2a and b.

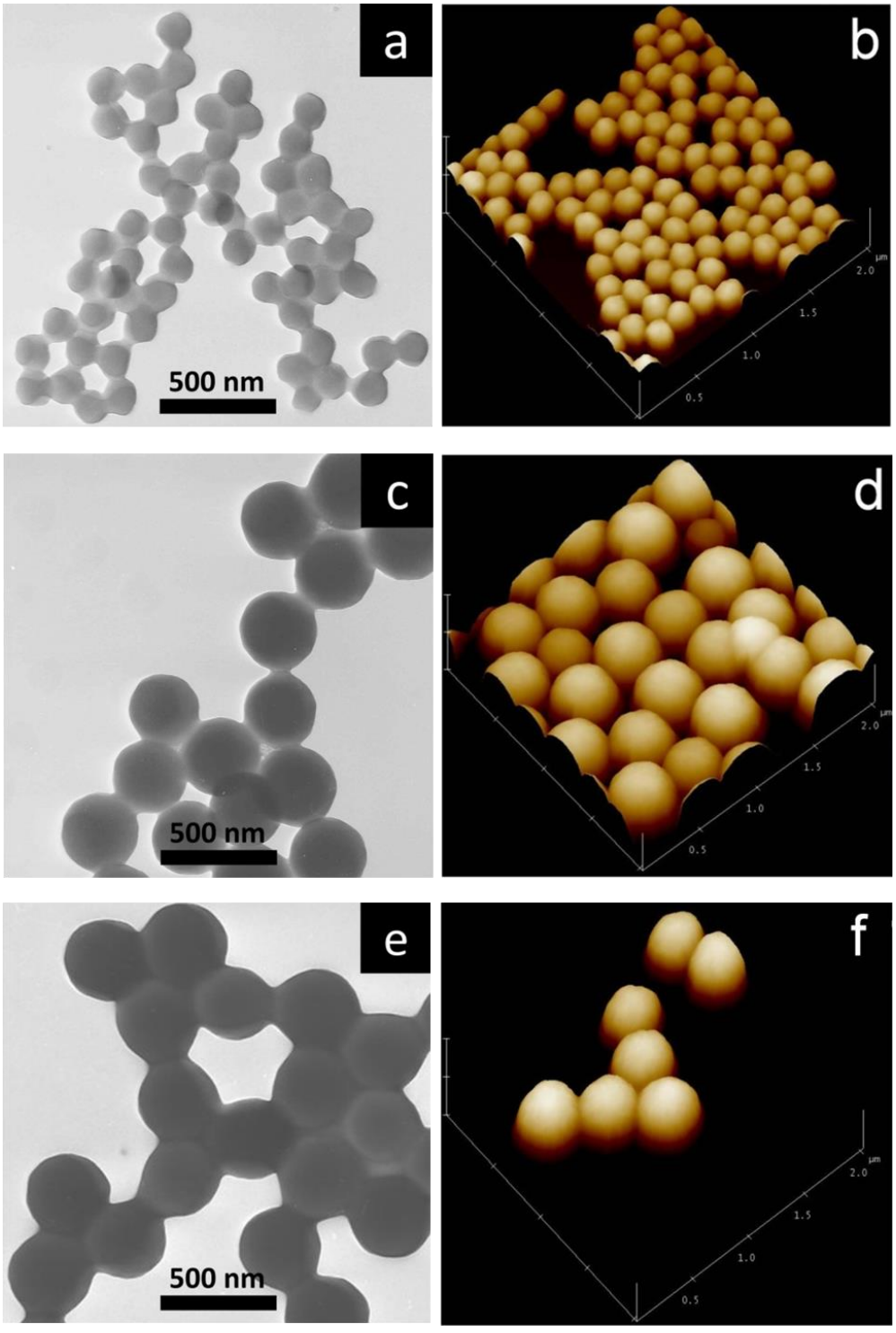

Figure 3-2 (a) *s*-GMA particles TEM image, (b) *s*-GMA particles AFM topography image, (c) *l*-GMA particles TEM image, (d) *l*-GMA particles AFM topography image, (e) *l*-NH2 particles TEM image, and (f) *l*-NH2 particles AFM topography image. AFM images Z range: 300 nm.

The diameters of the small epoxy-functionalized particles were also measured via DLS. DLS measurements yielded a hydrodynamic diameter (D_h) of 212 ± 2 nm and a PDI of 0.053, as summarized in Table 3-1. These particles had a low polydispersity, although the diameter measured via DLS was larger than that determined by TEM. In the case of TEM imaging, the particles were aero-sprayed from solution and left to dry before their images were recorded. In contrast, DLS measurements were performed in solution. Consequently, the final diameter obtained via DLS measurements incorporated a contribution from the layer of solvent molecules that had become adsorbed onto the particles.[65] The hydrodynamic diameter measured by DLS represents the scattering-intensity-average diameter, which is also known as the *z*-average diameter. Meanwhile, the diameter obtained from the TEM measurements corresponded to the number-average diameter.

Table 3-1 The hydrodynamic radius (D_h) and polydispersity indices (PDI) of the various particles.

Particle	D_h (nm)	PDI
Small PS-GMA Particles	212 ± 2	0.053 ± 0.021
Large PS-NH2 Particles	444 ± 5	0.050 ± 0.014
1:100 Raspberry-like Particles	648 ± 9	0.183 ± 0.008

In addition, the small PS-GMA particles were characterized via DRIFT-IR spectroscopy. The spectrum of the small PS-GMA particles shown in Figure 3-3 exhibits absorption peaks corresponding to the phenyl groups of PS at 3025 cm^{-1} (sp^2 C-H stretching, aromatic), 1600 cm^{-1} (C=C stretching, aromatic), 1493 and 1452 cm^{-1} (C-H bending, backbone), as well as at 760 and 700 cm^{-1} (C-H bending, aromatic). In addition, a peak corresponding to the C-H stretching of the methylene group was also observed at 2929 cm^{-1}.[47-49] Meanwhile, the absorption peak at 1729

cm^{-1} (C=O stretching) and the peaks at 1255 and 908 cm^{-1} (C-O stretching, epoxy groups) corresponded to the GMA units.[48-49] The co-existence of aromatic rings and epoxy groups suggests that the copolymerization of styrene and glycidyl methacrylate had proceeded successfully.

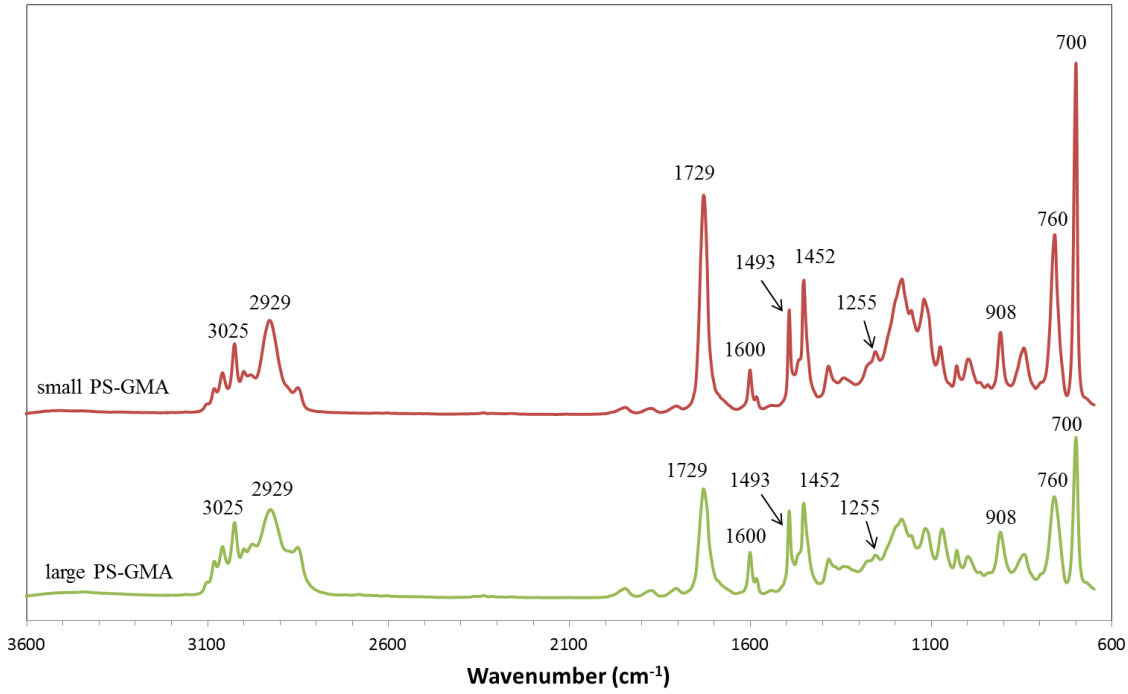

Figure 3-3 DRIFT-IR spectra of the small (top, red spectrum) and the large (bottom, green spectrum) PS-GMA particles.

3.2.2 Characterization of the Large Epoxy- and Amino-Functionalized Polystyrene Particles

The large PS-GMA particles were prepared via seeded emulsion polymerization. First, PS seed particles were prepared through the surfactant-free emulsion polymerization of St using V50 as the initiator and DVB as the crosslinking agent. To this reaction mixture were then added more of the St monomer, GMA as an epoxy-functional comonomer, and more of the DVB crosslinking agent. Seeded polymerization was employed to produce larger particles as well as to

ensure that the epoxy groups were located at the surfaces of these particles. Figure 3-2c and d show a TEM image as well as AFM images of the large PS-GMA particles. The particles were predominantly spherical and smooth, with an average TEM diameter of 332 ± 10 nm. The DRIFT-IR spectrum of the large epoxy-functionalized particles can be seen in Figure 3-3 at the bottom of the figure. As would be anticipated, this spectrum was very similar to that of the small PS-GMA particles since these particles had a similar chemical composition. Absorption signals corresponding to the phenyl groups of PS were observed at 3025, 1600, 1493, 1452, 760 and 700 cm^{-1}, while a signal observed at 2929 cm^{-1} corresponded to the C-H stretching of the methylene groups. In addition, absorption peaks corresponding to the GMA groups were also observed at 1729, 1255, and 908 cm^{-1}.

The large PS-GMA particles were then converted to the large PS-NH_2 particles via reaction with EDEA. The epoxy-groups on the surfaces of the large PS-GMA particles underwent ring-opening reactions with one of the terminal amino groups of EDEA, thus PS-NH_2 particles. In order to obtain well-dispersed large PS-NH_2 particles, the large PS-GMA particles were added drop-wise into a solution of EDEA. As a droplet of the particles reached the solution, EDEA would react with the epoxy groups on the surfaces of the particles and convert them into amino groups before the next droplet reaches the solution, thus preventing the particles from becoming crosslinked together. The corresponding TEM and AFM images of the resultant particles are shown in Figure 3-2e and f, and the particles had an average TEM diameter of 337 ± 10 nm. In addition, DLS measurements yielded a hydrodynamic diameter of 444 ± 5 nm and a PDI of 0.050. The polydispersity of these particles was low, and once again the diameter obtained via DLS measurements was larger than that obtained by TEM characterization.

A ninhydrin test was performed to verify the presence of the amino groups on the surfaces of the resultant particles.[53-54] These particles were added to an aqueous ninhydrin

solution at room temperature and heated for 2 min. The color of the solution changed from white to purple, as shown in Figure 3-4, indicating that amino groups were indeed present on the surfaces of the particles. Thus, it was apparent that the conversion of the epoxy groups into amino groups had proceeded successfully. In addition, the large PS-NH_2 particles were characterized via DRIFT-IR spectroscopy and a spectrum is shown in Figure 3-5. Absorption peaks corresponding to the epoxy groups that were observed at 1255 and 908 cm^{-1} decreased in intensity but still remained. This indicates that EDEA did not penetrate the large PS-GMA particles and only reacted with the epoxy groups on the surfaces of the particles. Meanwhile, the absorption peak corresponding to the carbonyl group was still observed at 1729 cm^{-1}, excluding the possibility of reactions taking place between EDEA and the ester groups of the GMA units. If the EDEA had reacted with the GMA ester groups in the manner shown in Figure 3-6, amide carbonyl signals would have appeared between 1650 cm^{-1} and 1670 cm^{-1}. However, no signals were observed in this region.

Figure 3-4 Photograph of vials containing small PS-NH_2 particles that were dispersed into distilled water (left) and into an aqueous ninhydrin solution (right).

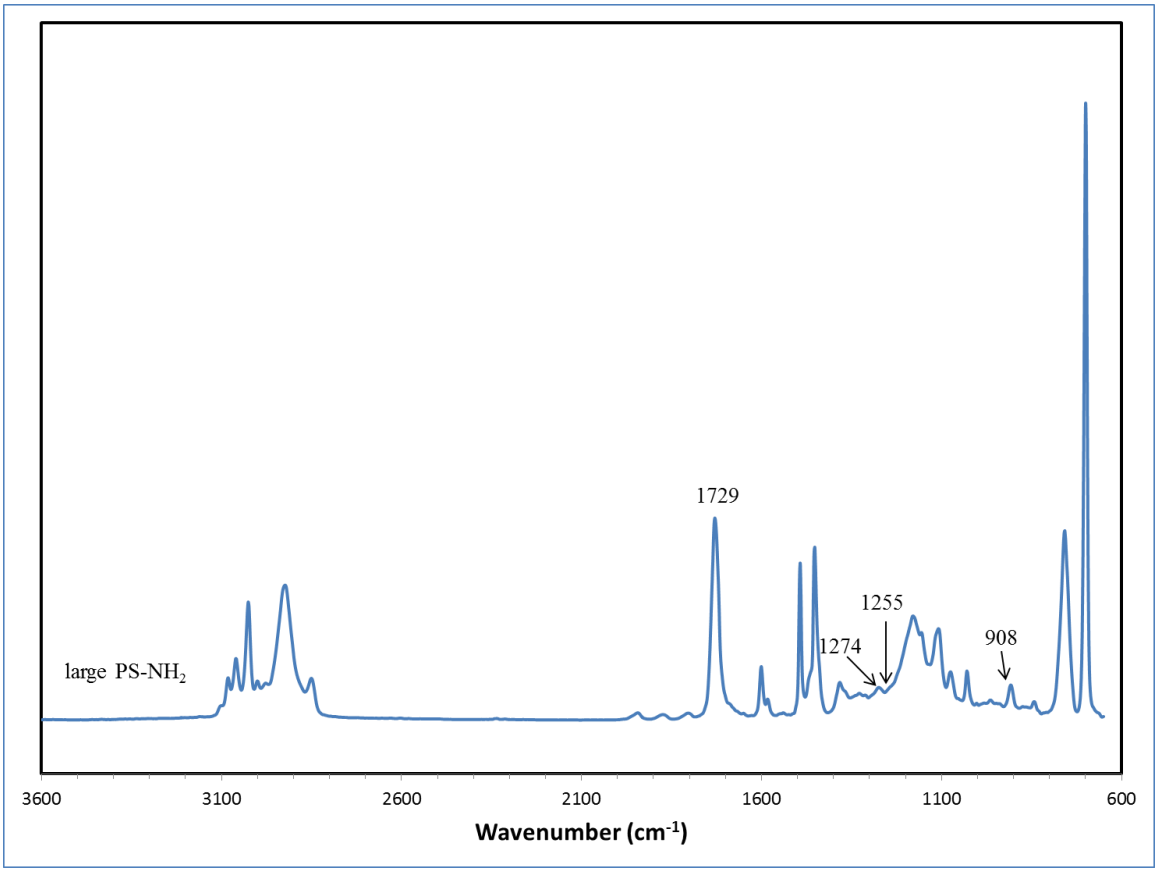

Figure 3-5 DRIFT-IR spectrum of a sample of large PS-NH_2 particles.

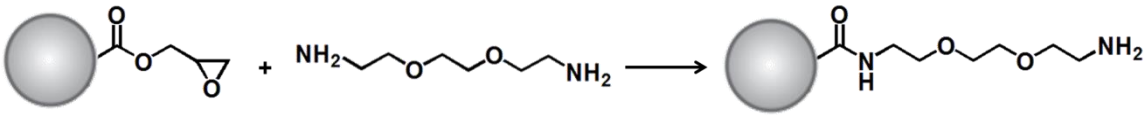

Figure 3-6 Possible reaction between EDEA and the ester group of a GMA unit on a particle surface.

3.3 Characterization of the Raspberry-Like Particles

Raspberry-like particles were fabricated by covalently binding the small PS-GMA particles with the large PS-NH_2 particles. These covalent bonds yielded stronger, more stable particle clusters than would be anticipated from non-covalent interactions. EDEA, a molecule

bearing primary amines at each end, was used to "glue" the small and large particles together. To accomplish this, EDEA was first attached to the large PS-GMA particles via an epoxy-amine ring-opening reaction to yield the large PS-NH_2 particles. Subsequently, these large PS-NH_2 particles were added drop-wise to a solution of the small PS-GMA particles. Multiple small PS-GMA particles reacted with each large PS-NH_2 particle once again via an epoxy-amine ring-opening reaction, resulting in well-defined raspberry-like particles that each consisted of a central large particle that was surrounded by many small particles. If the particle addition steps were reversed, with the small PS-GMA particles being added into a solution of the large PS-NH_2 particles, multiple large PS-NH_2 particles would react with each small PS-GMA particle. This would result in random aggregates of the particles incorporating more than one large particle. For example, two large particles could become connected through one small particle.

3.3.1 Calculation of the Maximum Theoretical Particle Coverage

The maximum theoretical number of small PS-GMA particles (N_{max}) covering one large amino-functionalized PS-NH_2 particle can be calculated geometrically. Assuming the small particles cover one of the large particles in a complete monolayer, the equatorial plane of the raspberry-like particles would resemble that illustrated in Figure 3-5a. Here, we can define a pseudo-large particle as a particle whose radius is the sum of the radii of one small particle and one large particle. If we cut the pseudo-large particle and spread its surface so that it assumed a flat geometry, as illustrated in Figure 3-5b, the top hemispheres of the small particles would be densely packed over the surface of the pseudo-large particle. A top-down view of the surface of such pseudo-large particle is shown in Figure 3-6. The circles that are densely packed in a hexagonal arrangement represent the projection area or the equatorial area of the small particles. It has been demonstrated that the highest density of circles can be achieved when they are

arranged in a hexagonal packing arrangement,[50] where each central circle is surrounded by six other circles, as illustrated in Figure 3-6. The surface area of one pseudo-large particle can be calculated from Equation 3.1, while the equatorial area of one small particle can be calculated using Equation 3.2. Meanwhile, the hexagonal packing parameter (η_h) is expressed by Equation 3.3. Through the use of the hexagonal packing parameter, the theoretical maximum number of the small particles N_{max} can be calculated geometrically using Equation 3.4:

$$A_1 = 4\pi(r_l + r_s)^2 \quad (3.1)$$

$$A_2 = \pi {r_s}^2 \quad (3.2)$$

$$\eta_h = \frac{\pi}{2\sqrt{3}} \quad (3.3)$$

$$N_{max} = \frac{\pi}{2\sqrt{3}}\frac{A_1}{A_2} = \frac{2\pi}{\sqrt{3}}\left(\frac{r_l + r_s}{r_s}\right)^2 \quad (3.4)$$

where r_l, r_s, and (r_l + r_s) correspond to the radii of large PS-NH_2 particles, small PS-GMA particles and pseudo-large particles, respectively.[51] Meanwhile, A_1 corresponds to the surface area of one pseudo-large particle and A_2 is the equatorial area of one small PS-GMA particle. N_{max} can then be estimated based on the radii obtained for the particles via TEM observation, which were found to be 168.5 nm for the large PS-NH_2 particles and 60 nm for the small PS-GMA particles. Thus, a maximum of 52 small PS-GMA particles can bind to one large PS-NH_2 particle from a geometrical point of view.

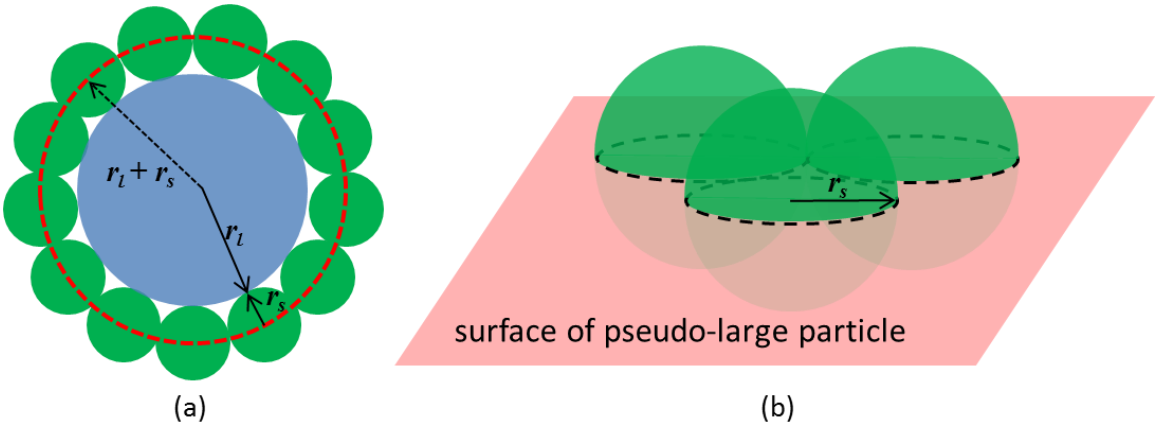

Figure 3-7 The equatorial plane of a raspberry-like particle is illustrated in (a), where the radius of a pseudo-large particle is indicated by the red dotted circle. The surface of a pseudo-large particle that has been projected over a flat surface is shown in (b), where the top halves of the small particles are densely packed on this surface.

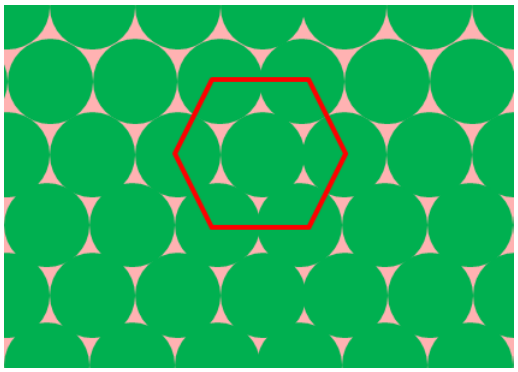

Figure 3-8 A top-down view of the surface of a pseudo-large particle bearing small particles that are densely packed in a hexagonal arrangement. Figure was taken out from a web source and modified.

3.3.2 Characterization of the 1:100 Raspberry-Like Particles

Raspberry-like particles were fabricated using a 1:100 number feed ratio of large amino-functionalized PS-NH_2 particles to small epoxy-functionalized PS-GMA particles. Variuos techniques, including TEM, SEM and AFM, were used to visualize the morphology of these

raspberry-like particles. Figure 3-7a, b, and c show the TEM, SEM, and AFM images of these particles. As the name implies, the particles adopted a raspberry-like morphology with each central large PS-NH_2 particle surrounded by multiple small PS-GMA particles. In general, the raspberry-like particles had not aggregated together, and the large PS-NH_2 particles were well-covered by the small PS-GMA particles. The average diameter of the raspberry-like particles measured from the TEM images was found to 565 ± 22 nm, while the diameter measured via SEM was 568 ± 25 nm. Both the TEM and SEM diameter measurements were performed by considering the average diameter of circles that would closely match the total diameter of each particle cluster indicated by the dotted circles in Figure 3-7a and b.

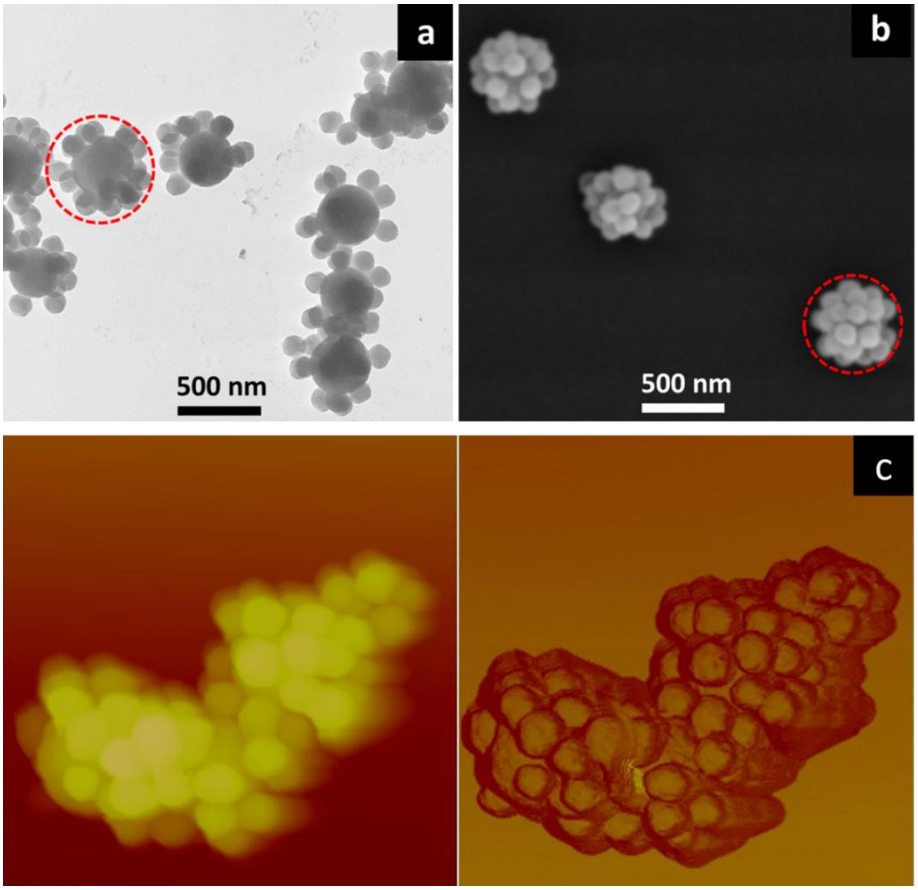

Figure 3-9 TEM (a), SEM (b), and AFM (c, topography at the left and phase at the right) images of 1:100 raspberry-like particles. AFM images: Size: 2 μm × 2 μm and Z range: 750 nm, 180°.

The DLS analysis provided a hydrodynamic radius of 648 ± 9 nm and a polydispersity index of 0.183. The DLS diameter value is once again larger than the diameter measured via TEM and SEM. As mentioned earlier, DLS measurements provide the *z*-average diameter and not the number-average diameter that is obtained via TEM or SEM. These raspberry-like particles were structurally complex. Consequently, they were not as uniform as the individual precursor particles due to small gaps in the structure between the attached small particles and the variation in the number of small particles that were attached to each large particle. The effect caused by the layer of solvent molecules adsorbed onto the particle also plays a role in the final diameter for this case.

3.3.3 Effect of the Large-to-Small Particle Number Feed Ratios on the Morphologies of the Raspberry-Like Particles

The effect of the number of small PS-GMA particles on the morphologies of the raspberry-like particles was investigated by varying the number feed ratio of the large PS-NH_2 particles to the small PS-GMA particles from 1:2 to 1:40. As was the case for the 1:100 raspberry-like particles, the large PS-NH_2 particles were added to a solution of the small PS-GMA particles in order to obtain well-defined raspberry-like particles with a large central particle surrounded by small particles. The geometrical maximum number of small particles that can bind to one large particle was previously calculated to be 52. Although this number describes the maximum capacity from a geometric perspective, there are many factors may affect the actual capacity, such as repulsive interactions between small particles.

TEM images of the raspberry-like particles that had been fabricated with large PS-NH_2 particle-to-small PS-GMA particle number feed ratios of 1:2 and 1:20 are shown in Figure 3-8a and b, respectively. These raspberry-like particles had formed aggregates and the individual

particles were not discernible. As the large PS-NH_2 particles were added to the solution of the small PS-GMA particles, multiple small PS-GMA particles reacted with each large PS-NH_2 particle. However, in both of these cases, the amount of small PS-GMA particles available was much lower than the geometrical maximum number of small particles that could bind to large particles. In particular, the number of small particles available was 4% and 38% of the geometric maximum when the number feed ratios of 1:2 and 1:20 were respectively employed. Thus, there was a greater chance for the small PS-GMA particles to react with more than one large particle, leading to coagulation of the resulting raspberry-like particles. The raspberry-like particles had formed aggregates in solution and the TEM samples were difficult to prepare in this instance, since the large aggregates would become stuck in the aero-spraying tube. As the number feed ratio was increased to 1:40, the number of small PS-GMA particles available was increased to a value 76% of the geometrical maximum. At this point, more small particles became available to react with the large particles and the bridging effect between large particles diminished significantly, as shown in Figure 3-8c. The raspberry-like particles were clearly visible in this TEM image and it was apparent that they had undergone less aggregation than the previous batch. In addition, the sample preparation for TEM imaging in this case was much more facile than for the previous cases, as expected. As the number of small PS-GMA particles was increased to exceed the geometrical maximum number of particles, the bridging effect diminished further. For further experiments, the raspberry-like particles were thus prepared at a large PS-NH_2 particle-to-small PS-GMA particles number feed ratio of 1:100.

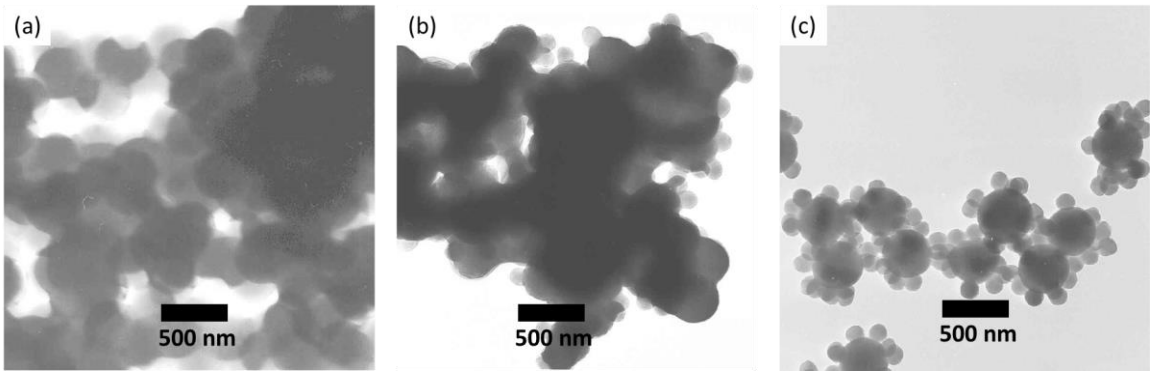

Figure 3-10 TEM images of raspberry-like particles prepared at large PS-NH_2 particle-to-small PS-GMA particle number feed ratios of 1:2 (a), 1:20 (b), and 1:40 (c), respectively.

Additionally, the bridging effect was demonstrated when the reaction time was shorten to 1 min (Figure 3-9). In this case, the large PS-NH_2 particles were rapidly mixed with the small PS-GMA particles at a 1:2 number feed ratio and left to react for 1 min before an excess of hexylamine was added to terminate the reactions between the particles. As a small molecule, hexylamine, could readily react with the epoxy groups on the surfaces of the small particles and convert them into hexyl groups, thus preventing further reactions between the large PS-NH_2 particles and the small PS-GMA particles. The TEM and AFM images shown in Figure 3-9 revealed that the large particles were bridged by the small particles. The observed bridging effect also demonstrated that the reaction between the two types of particles was very rapid, taking place in less than 1 min. This suggests that the total reaction time for fabricating the well-defined raspberry-like particles could be shortened instead of requiring an overnight reaction.

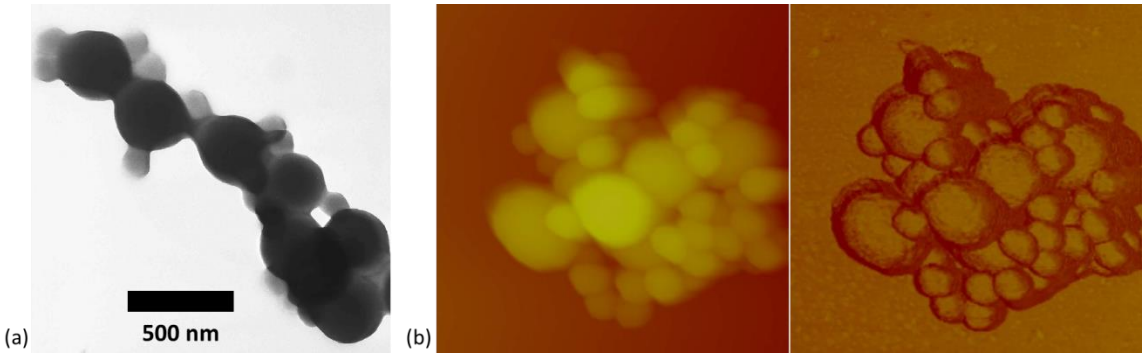

Figure 3-11 TEM (a) and AFM (b, topography at the left and phase at right) images of the product prepared at a 1:2 number feed ratio and with a 1 min reaction time. AFM images: Size: 2 μm × 2 μm and Z range: 750 nm, 180°.

3.4 Synthesis and Characterization of P(GMA-*co*-FOEMA)

Fluorinated polymers are suitable for many applications due to their enhanced water and/or oil repellency,[52-54] chemical and thermal stability,[55-56] as well as their low refractive indices.[57] For example, *n*-perfluoroeicosane exhibits a low surface tension of 6.7 mN/m,[58] and is thus an excellent candidate for enhancing the amphiphobicity of a surface. With this in mind, the fluorinated random copolymer P(GMA-*co*-FOEMA) was synthesized via ATRP. This polymer was targeted because the epoxy groups of the GMA units were able to react with the amino-groups of the raspberry-like particles, thus incorporating the fluorinated copolymer onto the surfaces of the raspberry-like particles. In addition, the FOEMA component would provide the particles with a low surface tension and thus enhance their amphiphobicity.

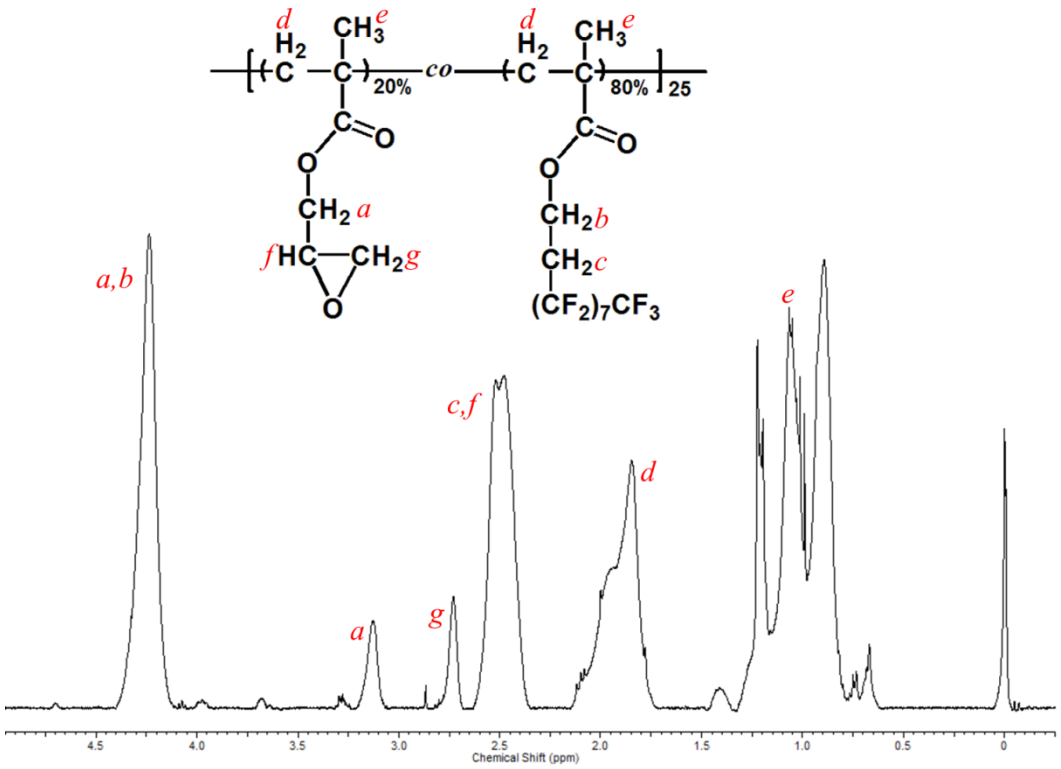

Figure 3-12 Structure and ^{1}H NMR spectrum of P(GMA-*co*-FOEMA), along with the corresponding peak assignments.

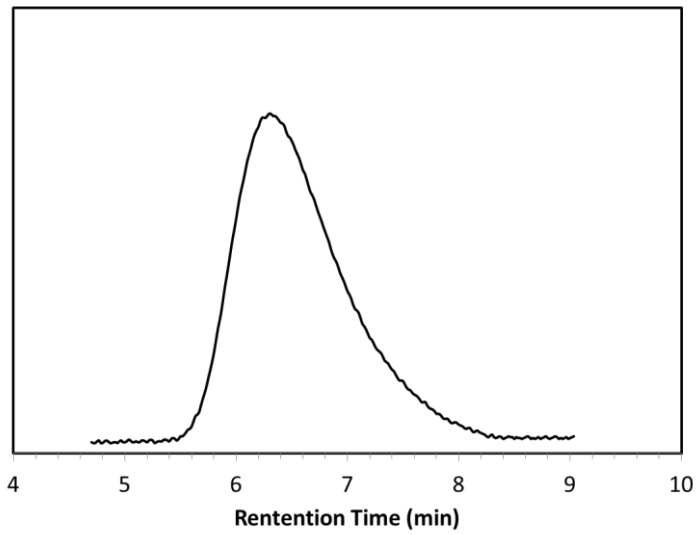

Figure 3-13 GPC trace of P(GMA-*co*-FOEMA).

The fluorinated copolymer P(GMA-*co*-FOEMA) has been characterized by ^{1}H NMR and by GPC. A ^{1}H NMR spectrum of the copolymer as well as the corresponding polymer peak assignments are shown in Figure 3-10. Peaks *b* and *g* were taken as representative resonances of protons from the FOEMA and GMA units, respectively. Peak *b* corresponded to two protons, while peak *g* corresponds to one proton, and the ratio between the integrations of peak *b* and *g* is 8:1 (*b*:*g*). Therefore, the ratio between the FOEMA and the GMA units is 4:1, indicating that the FOEMA components comprised 80 mol% of the copolymer. The signal intensity of the H-C-Br peak corresponding to the end group of the initiator located at 4.0 ppm in the ^{1}H NMR spectrum was compared to the signal intensity of peak *g* corresponding to the GMA unit in order to calculate the number of repeat units in the copolymer. Through the calculation, it was found that the copolymer possessed 5 GMA units and 20 FOEMA units, so that the copolymer had an overall repeat unit number of 25. In addition, a GPC trace for the copolymer is shown in Figure 3-11, where a single peak appears at 6.2 min. The number average molecular weight (M_n) and the polydispersity index (M_w/M_n) determined based on polystyrene standards were found to be 58,500 g/mol and 1.15, respectively. The molecular weight obtained via GPC was different from that obtained from ^{1}H NMR, since the polystyrene standards have different structures from the fluorinated copolymer.

3.5 Wettability of the Fluorinated Raspberry-Like Particle-Based Films

The 1:100 raspberry-like particles were functionalized with the fluorinated random copolymer P(GMA-*co*-FOEMA) and subsequently coated onto glass substrates. It was hoped that the combination of the low surface energy provided by the fluorinated copolymer and the dual-scale hierarchical surface roughness, as well as the re-entrant geometry provided by the raspberry-like particles would impart coated substrates with superamphiphobic properties. After

the fluorinated raspberry-like particles were prepared and purified, they were dispersed into TFT. These dispersions were then cast onto a glass slide and subsequently evaporated, thus coating the glass slide. For comparison, two glass slides were also coated with P(GMA-*co*-FOEMA) alone and with fluorinated small particles, respectively.

AFM images of glass slides that were coated with P(GMA-*co*-FOEMA), fluorinated small particles, and fluorinated raspberry-like particles are shown in Figure 3-12a, b, and c, respectively. The root-mean-square roughness (rms) was measured for these surfaces with AFM imaging software for different regions of the samples. In the case of the film that was composed of the fluorinated copolymer alone, the rms value was 0.83 ± 0.7 nm, which was indicative of a flat surface. The rms value for the fluorinated small particle-based film was 51 ± 7 nm, as expected for a much rougher surface. Finally, the rms value for the fluorinated raspberry-like particle-based film was 102 ± 16 nm, indicating this coating had the greatest degree of roughness. The SEM images showed that these particles coated the glass substrates in multiple layers and a few cracks were observed between particle clusters. Thus, surface roughness was enhanced by this packing behavior. In addition, the film that was coated with the fluorinated raspberry-like particles was more complex and exhibited a rougher morphology than the film that was composed of the fluorinated small particles. A dual-scale hierarchical surface roughness was clearly visible in the SEM image of the glass substrate that was coated with the fluorinated raspberry-like particle-based film. In particular, a larger scale of roughness was observed between raspberry-like complex particles, while a smaller scale of roughness was observed between the small particles that were located on the surfaces of each individual raspberry-like particle. As mentioned in Chapter 1, the re-entrant geometry could exist in both of the two films that were coated with the fluorinated particles. This was especially the case for the fluorinated raspberry-like particle-base film, as a re-entrant geometry exhibited not only on the bottom halves of the

raspberry-like particles themselves, but were also present on the on the bottom halves of the small particles that were located on the surface of each individual raspberry-like complex particle.

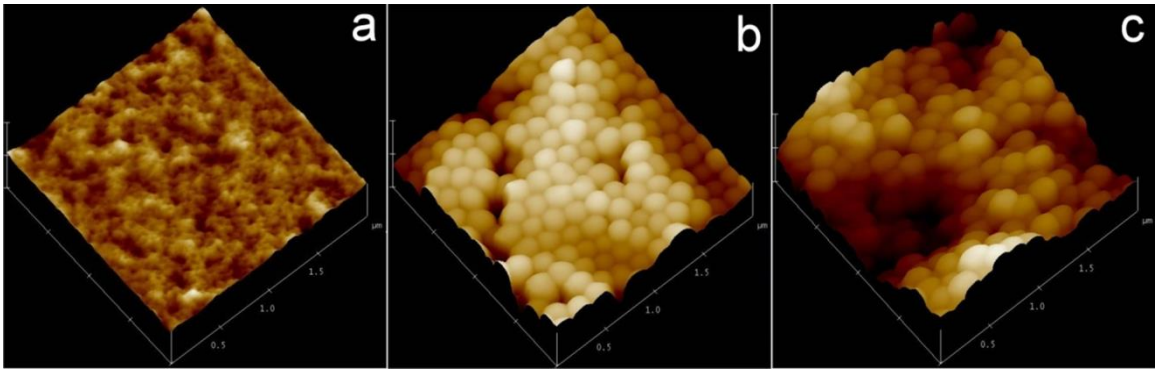

Figure 3-14 AFM topography images of coatings of (a) P(FOEMA-co-GMA), Z range: 30 nm, (b) fluorinated small particles, Z range: 300 nm, and (c) fluorinated raspberry-like particles on glass plates, Z range: 300 nm.

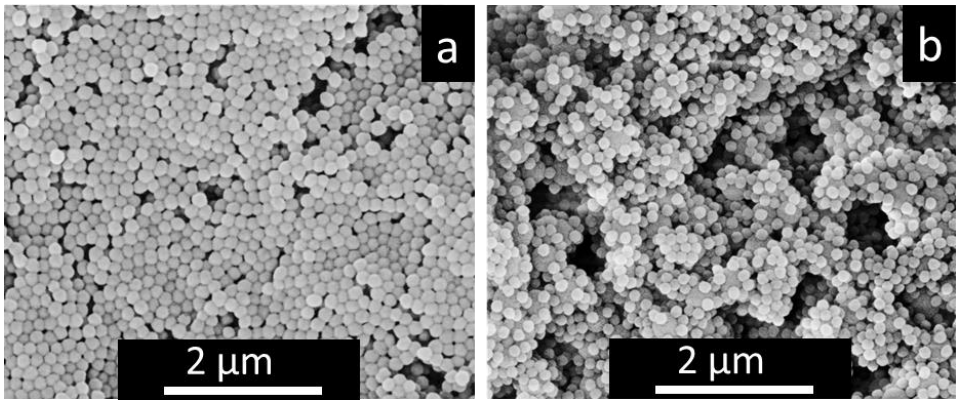

Figure 3-15 SEM images of coatings of (a) fluorinated small particles and (b) fluorinated raspberry-like particles.

The wettability of these films was characterized via static contact angle, sliding angle and shedding angle measurements, using deionized water and various oil droplets as test liquids. In

particular, diiodomethane, cooking oil, and hexadecane were used as the oil droplets. Photographs of water droplets placed onto glass slides that had been coated with fluorinated copolymer, the fluorinated small particles and with the fluorinated raspberry-like particles are shown in Figure 3-14a, b, and c, respectively. The static contact angle increased from $121 \pm 2°$, to $148 \pm 5°$, to $165 \pm 2°$ as the coating was respectively changed from the smooth fluorinated copolymer-based film, to the fluorinated small particle-based film, and to fluorinated raspberry-like particle-based film. The static water contact angle exhibited by the smooth fluorinated copolymer-based film was very similar to the average water contact angle of $119°$ that had been reported in literature for the smooth *n*-perfluoroeicosane-coated surfaces.[58] The results of these static water contact angle tests, along with the results of the water sliding and water shedding angle tests of these films are summarized in Table 3-2. Sliding angle tests were not performed on the smooth fluorinated copolymer-based film because the water droplets did not roll off of these surfaces, even when they were tilted to $90°$. The GMA units of the copolymer could undergo hydrogen bonding interactions with the water droplet, thus causing the droplet to remain in place. However, when water droplets were dropped onto the surfaces during the shedding angle measurements, the water droplets rolled off of the surfaces when they were tilted at a $45°$ angle. This difference in performance could be attributed to the initial energy provided to the droplet as it impacted the surface, which may have been sufficient to overcome the GMA-water hydrogen bonding interactions. The fluorinated raspberry-like particle-based films showed enhanced performance in these measurements too, displaying water sliding angles and water shedding angles that were both less than $1°$ indicated a superhydrophobic surface. The low sliding angle, taken in combination with the high static contact angle, indicated that the fluorinated raspberry-like particle-based films were indeed superhydrophobic. Nevertheless, superhydrophobic raspberry-like particle-based films have been prepared previously by Ming et al.[41] and by Qian et al.[59] The films based on poly(dimethylsiloxane)-modified raspberry-like particles prepared by

Ming and coworkers exhibited a water contact angle of 165 ± 1 ° and a sliding angle of 3 ± 1 °,[41] while those prepared by Qian et al. and based on dodecyltrichlorosilane-modified raspberry-like particles exhibited a water contact angle of 162 ° and a sliding angle of 3 °.[59]

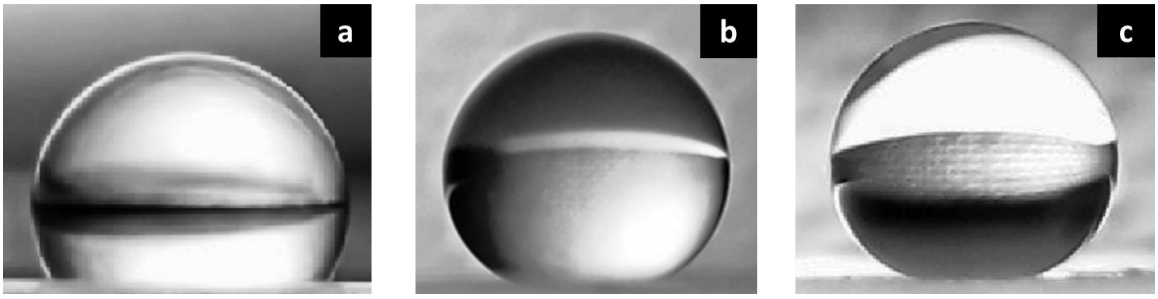

Figure 3-16 Photographs of deionized water droplets sitting on glass substrates that had been coated with fluorinated copolymer (a), fluorinated small particles (b), and fluorinated raspberry-like particles (c). The contrast in each of these photographs was adjusted using the Image J software package, and the patterns observed on the droplets were due to the reflection of the background used when taking these photos. A similar treatment was applied to the photographs shown in Figure 3-14.

Table 3-2 Static water contact, sliding, and shedding angles that have been obtained for glass substrates that have been coated with the fluorinated copolymer, with the fluorinated small particles, and with the fluorinated raspberry-like particles.

Liquid	Static contact angle ( )	Sliding angle ( )	Shedding angle ( )
		Fluorinated copolymer	
Water	121 ± 2	N/A[a]	45 ± 2
		Fluorinated small particles	
Water	148 ± 5	< 1	< 1
		Fluorinated raspberry-like particles	
Water	165 ± 2	< 1	< 1

[a]No sliding angle was recorded. The water droplet did not roll off the material and remained attached to the sample even at a tilting angle of 90°.

A surface can be provided with superhydrophobic properties through the incorporation of an appropriate degree of surface roughness, re-entrant geometry and a low surface tension.[40] One method of introducing superhydrophobicity to a surface is to coat it with hierarchically-structured particles that had been modified with a fluorinated polymer. As has been demonstrated in this work and by other researchers,[4,59] these films can be fabricated using raspberry-like particles consisting of small spheres that are attached to larger spheres, yielding a film which possesses a surface roughness at both nano- and micro-scale. The high contact angles displayed by these superhydrophobic films can be explained using the Cassie-Baxter model.[60] In this model, the water droplet does not come into full contact with the surface due to air pockets that are trapped between the droplet and the rough surface. Consequently, the measured contact angle takes into account the interactions between the liquid droplet, the solid surfaces and the air pockets. Functionalized raspberry-like particles, with their dual-scale surface structures and low surface tension, have been shown in the literature to facilitate this Cassie-Baxter behavior and thus provide substrates with superhydrophobic properties.[24,41] In our case, as the smooth fluorinated copolymer-based coating was replaced with the fluorinated small particles, and finally with the fluorinated raspberry-like particles, the surface became increasingly complex and rough. As the degree of structural complexity and roughness increased, more air bubbles would become trapped between the droplet and the surface. Consequently, the substrate that was coated with fluorinated raspberry-like particles and provided with the greatest degree of roughness was driven into the superhydrophobic regime.

From a practical aspect, a superamphiphobic surface simultaneously possessing both superhydrophobic and superoleophobic properties would have many advantages. A superoleophobic surface has a contact angle greater than 150 ° and a sliding angle of less than 10^{o} with oils.[35] We investigated the oil repellency of three fluorinated copolymer-modified surfaces by measuring the static contact angle, sliding angle and shedding angles, using various oil

droplets including diiodomethane, cooking oil and hexadecane as the test liquids. As was the case with the water-repellency tests described above, the three fluorinated copolymer-based surfaces included glass slides that had been coated with fluorinated copolymer itself, with fluorinated small particles, and with fluorinated raspberry-like particles. Photographs recorded during the static contact angle tests on these three substrates showing images of diiodomethane, cooking oil, and hexadecane droplets are shown in Figure 3-15a, b, and c, respectively. The contact angles obtained during these tests with the oil droplets are summarized in Table 3-3. As the structural complexity and roughness of the coating increased, the static contact angles of these oils generally increased as well, while the sliding and shedding angles decreased.

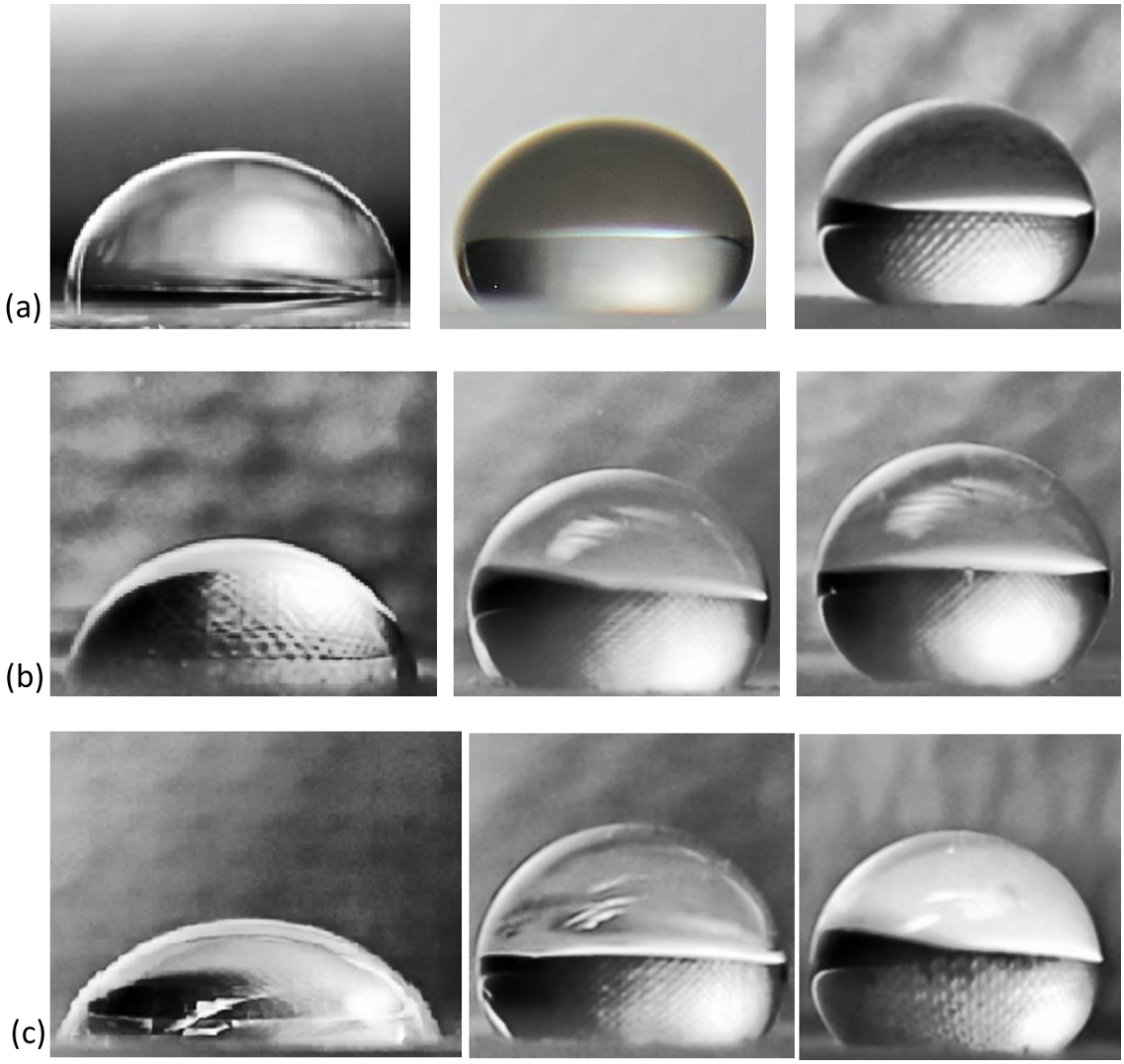

Figure 3-17 Photographs of various oil droplets, including diiodomethane (a), cooking oil (b), and hexadecane (c), that were recorded during static contact angle tests. The surfaces tested included glass substrates that had been coated with the fluorinated copolymer (left images), with fluorinated small particles (center images), and with fluorinated raspberry-like particles (right images).

Table 3-3 Static contact, sliding and shedding angles obtained using oil droplets for glass substrates that haven been coated with the fluorinated copolymer, with fluorinated small particles, and with fluorinated raspberry-like particles.

Liquid	Static contact angle (°)	Sliding angle (°)	Shedding angle (°)
		Fluorinated copolymer	
Diiodomethane	95 ± 1	15 ± 3	12 ± 1
Cooking oil	90 ± 1	35 ± 1	35 ± 1
Hexadecane	72 ± 3	17 ± 2	17 ± 2
		Fluorinated small particles	
Diiodomethane	138 ± 2	6 ± 1	4 ± 1
Cooking oil	136 ± 3	N/A[a]	N/A
Hexadecane	132 ± 2	N/A[a]	N/A
		Fluorinated raspberry-like particles	
Diiodomethane	155 ± 3	< 1	< 1
Cooking oil	152 ± 4	7 ± 2	7 ± 2
Hexadecane	143 ± 1	13 ± 2	13 ± 2

[a]No sliding and shedding angles were recorded for these sample. The cooking oil or hexadecane droplets did not roll off the surface when it was titled at 90 °.

The static contact angles measured for these surfaces using diiodomethane increased from 95 ± 1 ° to 138 ± 2 ° to 155 ± 3 °, respectively, as tests proceeded from the substrates that were coated with the fluorinated copolymer, to those coated with fluorinated small particles, and finally to those that were coated with fluorinated raspberry-like particles. Meanwhile, the sliding and shedding angles decreased to less than 1 ° as the coating became increasingly rough, indicating that the fluorinated raspberry-like particle-based film was indeed oil-repellent. In

addition, the static contact angle measured for the three fluorinated surfaces using cooking oil, a more common chemical encountered in everyday applications, increased from $90 \pm 1°$, to $136 \pm 3°$, and to $152 \pm 4°$ as the coating became increasingly rough. Meanwhile, both the sliding and shedding angles decreased to $7 \pm 2°$ when the films were based on the fluorinated raspberry-like particles. Moreover, hexadecane exhibited static contact angles that increased from $72 \pm 3°$, to $132 \pm 2°$, and to $143 \pm 1°$ as the coating became increasingly rough. Meanwhile the sliding and shedding angles of the hexadecane droplets decreased to $13 \pm 2°$ as the tests proceeded toward the fluorinated raspberry-like particle-based film.

As mentioned earlier, it can be more difficult to prepare a superoleophobic surface than a superhydrophobic surface, since many oils exhibit a lower surface tension than water. As the surface tensions of various liquids decreases from 72.9, to 50.9, to 33.8, and to 27.5 mN/m, respectively, for water,[61] diiodomethane,[62] cooking oil,[63] and hexadecane,[61] the corresponding contact angles of these droplets would also decrease. This trend was also observed in our case for the three types of fluorinated copolymer-based films. The fluorinated raspberry-like particle-based film showed superoleophobic behavior against both diiodomethane and cooking oil droplets. Meanwhile, this surface only exhibited highly oleophobic behavior against hexadecane, rather than superoleophobic behavior. However, the low value recorded for the sliding angle indicated that hexadecane was still readily repelled by this surface.

The Cassie-Baxter model can be employed once again to understand the superoleophobic behavior exhibited by the raspberry-like particles. An oil droplet may rest above the gaps on a rough surface, thus trapping air within these void spaces. As was the case with the water droplets, these trapped air pockets would prevent the oil droplet from coming into full contact with the surface of the rough substrate, resulting in a high contact angle. However, the fluorinated small particle-based film no longer satisfied the Cassie-Baxter model in the cases of the cooking oil and

hexadecane droplets. These droplets would penetrate into the void spaces between these particles, thus forcing the transition from the Cassie-Baxter state to the Wenzel state.[64] The liquid would have to recede from these pockets before the droplet could roll off the surface. However, this transition from the Wenzel state back to the Cassie-Baxter state has a high energy barrier.[35-36] This irreversibility derives from the fact that the dewetting process requires a desorption of the liquid from the solid surface and a substantial activation energy.

The films based on the complex fluorinated raspberry-like particles described in this thesis exhibited enhanced repellency against both water and oil droplets, and it was demonstrated that they possessed superamphiphobic properties. If water or oil comes into contact with these hierarchically structured fluorinated materials, the droplets will readily roll off the material and leave behind a clean surface. As mentioned earlier in this thesis, self-cleaning surfaces are highly desirable for a wide range of applications.[65,67] While these materials have great potential for various applications, the preparation of these surfaces remains challenging and many factors can influence their performance. The key requirements include a low surface tension, hierarchical roughness, as well as the availability of re-entrant sites. The fluorinated particle-based films described in this thesis appear to have met these requirements. Nevertheless, it may be possible to enhance the performance of these materials further through the careful optimization of various parameters. Varying the dimensions of the building blocks of these hierarchical surfaces, notably the sizes of both the small and the large particles, may help enhance the superamphiphobicity of the resultant films. In addition, the degree of fluorination may provide another area where further optimization is possible.

References

1. Langer, R.; Tirrell, D. A., *Nature* **2004,** *428*, 487-492.
2. Kohler, D.; Madaboosi, N.; Delcea, M.; Schmidt, S.; De Geest, B. G.; Volodkin, D. V.; Möhwald, H.; Skirtach, A. G., *Adv. Mater.* **2012,** *24*, 1095-1100.
3. McConnell, M. D.; Kraeutler, M. J.; Yang, S.; Composto, R. J., *Nano Lett.* **2010**, *10*, 603-609.
4. Zhang, J.-T.; Chao, X.; Asher, S. A., *J. Am. Chem. Soc.* **2013,** *135*, 11397-11401.
5. Gangwal, S.; Pawar, A. B.; Kretzschmar, I.; Velev, O. D., *Soft Matter* **2010,** *6*, 1413-1418.
6. Pawar, A. B.; Kretzschmar, I., *Macromol. Rapid Commun* **2010,** *31*, 150-168.
7. Yi, G.-R.; Pine, D. J.; Sacanna, S., *J. Phys.:Condens. Matter.* **2013,** *25*, 193101.
8. Hong, L.; Jiang, S.; Granick, S., *Langmuir* **2006,** *22*, 9495-9499.
9. Schmid, A.; Tonnar, J.; Armes, S. P., *Adv. Mater.* **2008,** *20*, 3331-3336.
10. Yuhong, Z.; Qichao, Z.; Xingwang, S.; Qingqiong, T.; Min, C.; Limin, W., *J. Colloid Interface Sci.* **2009,** *336*, 544-550.
11. Fan, X.; Zheng, L.; Cheng, J.; Xu, S.; Wen, X.; Cai, Z.; Pi, P.; Yang, Z., *Surf. Coat. Technol.* **2012,** *213*, 90-97.
12. Yake, A. M.; Snyder, C. E.; Velegol, D., *Langmuir*, **2007**, *23*, 9069-9075.
13. Li, G.; Yang, X.; Wang, J., *Colloids Surf. A: Physicochem. Eng. Aspects*, **2008**, *322*, 192-198.
14. de Gennes, P. G., *Science*, **1992**, *256*, 495-497.
15. Walther, A.; Müller, A. H. E., *Chem. Rev.*, **2013**, *113*, 5194-5261.
16. Saito, N.; Liu, C.; Lodge, T. P.; Hillmyer, M. A., *Macromolecules*, **2008**, *41*, 8815-8822.
17. Moughton, A. O.; Hillmyer, M. A.; Lodge, T. P., *Macromolecules*, **2012**, *45*, 2-19.
18. Perro, A.; Reculusa, S.; Bourgeat-Lami, E.; Duguet, E.; Ravaine, S., *Colloids Surf. A: Physicochem. Eng. Aspects*, **2006**, *284-285*, 78-83.
19. Puretskiy, N.; Ionov, L., *Langmuir*, **2011**, *27*, 2006-3011.
20. Zhou, X.; Shao, H.; Liu, H., *Colloid. Polym. Sci.*, **2013**, *291*, 1181-1190.
21. Barthlott, W.; Neinhuis, C., *Planta*, **1997**, *202*, 1-8.
22. Gao, X.; Jiang, L., *Nature*, **2004**, *432*, 36.
23. Gao, L.; McCarthy, T. J., *Langmuir*, **2006**, *22*, 2966-2967.
24. Celia, E.; Darmanin, T.; Taffin de Givenchy, E.; Amigoni, S.; Guittard, F., *J. Colloid Interface Sci.*, **2013**, *402*, 1-18.
25. Yao, X.; Song, Y.; Jiang, L., *Adv. Mater.*, **2011**, *23*, 719-734.
26. McHale, G.; Shirtcliffe, N. J.; Aqil, S.; Perry, C. C.; *Phys. Rev. Lett.*, **2004**, *93*, 036102.
27. Butt, H.-J.; Semprebon, C.; Papadopoulos, P.; Vollmer, D.; Brinkmann, M.; Ciccotti, M., *Soft Matter*, **2013**, *9*, 418-428.
28. Yuan, Z.; Xiao, J.; Wang, C.; Zheng, J.; Xing, S.; Liu, J., *J. Coat. Technol. Res.*, **2011**, *8*, 773-777.
29. Valipour Motlagh, N.; Birjandi, F. Ch.; Sargolzaei, J.; Shahtahmassebi, N., *Appl. Surf. Sci.*, **2013**, *283*, 636-647.
30. Perreira, C.; Alves, C.; Monteiro, A.; Magén, C.; Pereira, A. M.; Ibarra, A.; Ibarra, M. R.; Tavares, P. B.; Araújo, J. P.; Blanco, G.; Pintado, J. M.; Carvalho, A. P.; Pires, J.; Pereira, M. F. R.; Freire, C., *ACS Appl. Mater. Interfaces*, **2011**, *3*, 2289-2299.
31. Zhou, H.; Wang, H.; Niu, H.; Gestos, A.; Lin, T., *Adv. Funct. Mater.*, **2013**, *23*, 1664-1670.
32. Xiong, D.; Liu, G.; Duncan, E. J. S., *Langmuir*, **2012**, *28*, 6911-6918.
33. He, Z.; Ma, M.; Lan, X.; Chen, F.; Wang, K.; Deng, H.; Zhang, Q.; Fu, Q., *Soft Matter*, **2011**, *7*, 6435-6443.
34. Geng, Z.; He, J.; Xu, L.; Yao, L., *J. Mater. Chem. A*, **2013**, *1*, 8721-8724.
35. Tuteja, A.; Choi, W.; Ma, M.; Mabry, J. M.; Mazzella, S. A.; Rutledge, G. C.; McKinley, G. H.; Cohen, R. E., *Science*, **2007**, *318*, 1618-1622.

36. Tuteja, A.; Choi, W.; Mabry, J. M.; McKinley, G. H.; Cohen, R. E., *Proc. Natl. Acad. Sci. USA*, **2008**, *105*, 18200-18205.
37. Zhao, H.; Law, K.-Y.; Sambhy, V., *Langmuir*, **2011**, *27*, 5927-5935.
38. Zhao, H.; Park, K.-C.; Law, K.-Y., *Langmuir*, **2012**, *28*, 14925-14934.
39. Leng, B.; Shao, Z.; de With ,G.; Ming, W. *Langmuir*, **2009**, *25*, 2456-2460.
40. Deng, X.; Mammen, L.; Butt, H.-J.; Vollmer, D. *Science*, **2012**, *335*, 67-70.
41. Ming, W.; Wu, D.; van Benthem, R.; de With. G., *Nano Lett.*, **2005**, *5*, 2298-2301.
42. Kling, J. A.; Ploehn, H. J., *J. Polym. Sci. A: Polym. Chem.*, **1995**, *33*, 1107-1118.
43. Lv, J.-N.; Fang, S.-J.; Chen, L., *Chin. J. Polym. Sci.*, **2009**, *27*, 101-108.
44. Cha, Y.-J.; Choe, S., *J. Appl. Polym. Sci.*, **1995**, *58*, 147-157.
45. Mouaziz, H.; Larsson, A.; Sherrington, D. C., *Macromolecules*, **2004**, *37*, 1319-1323.
46. Zurkova, E.; Bouchal, K.; Zdenkova, D.; Pebzbauer, Z.; Svec, F.; Kalal, J., *J. Polym. Sci.: Polym. Chem. Ed.*, **1983**, *21*, 2949-2960.
47. Liang, C. Y.; Krimm, S., *J. Polym. Sci.*, **1958**, *27*, 241-254.
48. Zeng, Z.; Yu, J.; Guo, Z.-X., *J. Polym. Sci. A: Poly. Chem.*, **2004**, *42*, 2253-2262.
49. Stuart, B. H., John Wiley & Sons: Chichester, UK, 2004.
50. Chang, H. C.; Wang, L. C., *Mathematics: Metric Geometry* **2010**.
51. Minami, H.; Mizuta, Y.; Suzuki, T., *Langmuir*, **2013**, *29*, 554-560.
52. Ameduri, B.; Boutevin, B.; Kostov, G., *Prog. Polym. Sci.*, **2001**, *26*, 105-187.
53. Xiong, D.; Liu, G.; Hong, L.; Duncan, E. J. S., *Chem. Mater.*, **2011**, *23*, 4357-4366.
54. Xiong, D.; Liu, G.; Duncan, E. J. S., *ACS Appl. Mater. Interfaces*, **2012**, *4*, 2445-2454.
55. Yang, Y.-W.; Hentschel, J.; Chen, Y.-C.; Lazari, M.; Zeng, H.; van Dam, R. M.; Guan, Z., *J. Mater. Chem.*, **2012**, *22*, 1100-1106.
56. Zhang, X.; Cao, G.; Sun, Z.; Xia, Z., *J. Appl. Phys.*, **2010**, *108*, 064113.
57. Lee, J. R.; Jin, F. L.; Park, S. J.; Park, J. M., *Surf. Coat. Technol.*, **2004**, *180*, 650-654.
58. Nishino, T.; Meguro, M.; Nakamae, K.; Matsushita, M.; Ueda, Y., *Langmuir*, **1999**, *15*, 4321-4323.
59. Qian, Z.; Zhang, Z.; Song, L.; Liu, H., *J. Mater. Chem.*, **2009**, *19*, 1297-1304.
60. Cassie, A. B. D.; Baxter, S., *Trans. Faraday Soc.*, **1944**, *40*, 546-550.
61. Jasper, J. J., *J. Phys. Chem. Ref. Data*, **1972**, *1*, 841-1009.
62. Korosi, G.; Kovats, E. S., *J. Phys. Chem. Ref. Data*, **1981**, *26*, 323-332.
63. Esteban, B.; Riba, J.-R.; Baquero, B.; Puig, R.; Rius, A., *Fuel*, **2012**, *102*, 231-238.
64. Wenzel, R. N., *Ind. Eng. Chem.*, **1936**, *28*, 988-994.
65. Martell, D. R. D.; Briones, J. R.; Hurtado, M. G.; López, A. d. R.; Meneses, V. M. C., *Materials Research* **2009,** *12*, 405-410.
66. Bhushan, B.; Jung, Y. C. *Prog. Mater. Sci.* **2011,** *56*, 1-108.
67. Liu, K.; Tian, Y.; Jiang, L. *Prog. Mater. Sci.* **2013,** *58*, 503-564.

Chapter 4

Summary and Conclusions

4.1 Fabrication of the Raspberry-Like Polymer Particles

In this thesis, small PS-GMA particles were prepared by the surfactant-free emulsion polymerization of St with GMA using V50 as the initiator and DVB as the crosslinking agent. Meanwhile, large PS-GMA particles were prepared via seeded emulsion polymerization. First, PS seed particles were prepared through the surfactant-free emulsion polymerization of St using V50 as the initiator and DVB as the crosslinking agent. To this reaction were then added more of St, GMA, and DVB. Subsequently, the large PS-GMA particles were then converted into the large PS-NH_2 particles via ring-opening reactions with EDEA. The sizes and morphologies of these precursor particles were carefully characterized via TEM, AFM, SEM, and DLS. In addition, DRIFT-IR spectroscopy and ninhydrin tests have been employed to detect the presence of epoxy groups and amino groups, respectively.

The raspberry-like polystyrene particles were successfully prepared through a ring-opening reaction between the exposed epoxy groups of the small 120 nm PS-GMA particles and the amine groups of the large 337 nm PS-NH_2 particles. The final morphologies of the raspberry-like particles could be controlled by adjusting the number feed ratio between the small epoxy-functionalized polystyrene particles and the large amino-functionalized polystyrene particles. Very little aggregation between the raspberry-like particles was observed when a number feed ratio of 1:100 between large and small particles was used, which closely matched the geometrically calculated maximum number of small particles that could be accommodated by one large particle. In addition, the use of this ratio yielded raspberry-like particles exhibiting a good coverage of the individual large particles by the small particles. The raspberry-like particles prepared under these conditions had a diameter of 565 ± 22 nm.

4.2 Superamphiphobic Coatings based on Fluorinated Raspberry-Like Particles

While the structure of these raspberry-like particles provided a dual-scale hierarchical roughness and re-entrant sites, they were further functionalized with a fluorinated random copolymer P(GMA-*co*-FOEMA) to provide them with a low surface tension. Subsequently, these fluorinated raspberry-like particles were cast onto glass slides to prepare the superamphiphobic coatings. These coatings exhibited a static contact angle of $165 \pm 2°$ and a sliding angle of less than $1°$ when they were tested against water, thus demonstrating that these films fell in the superhydrophobic regime. Additionally, the oil-repellency of these coatings was tested against various liquids, including diiodomethane, cooking oil, and hexadecane. The coatings exhibited superoleophobic behavior against diiodomethane and cooking oil, with respective static contact angles of $155 \pm 3°$ and $152 \pm 4°$. Both the sliding and shedding contact angles of these coatings were similar, and these coatings exhibited angles of $< 1°$ and $7 \pm 2°$ against diiodomethane and cooking oil, respectively. In the case of hexadecane, the recorded static contact angle was $143 \pm 1°$, while the sliding and shedding angles were both $13 \pm 2°$. Although this coating no longer fell under the superoleophobic regime when it was tested against hexadecane, it still exhibited highly oleophobic behavior against this liquid.

4.3 Significance of this Work

Superamphiphobic materials have generated significant interest due to their great potential as self-cleaning surfaces that can protect surfaces against corrosion, bacteria, fog, ice, and other forms of contamination.[1-2] However, the preparation of superamphiphobic surfaces is very difficult to achieve due to the need for hierarchical roughness, re-entrant sites, and a very low surface tension.[3-8] It should be noted that there have been no reports describing the

preparation of superamphiphobic coatings with comparable performance through self-assembly techniques.

We have successfully prepared superamphiphobic coatings through a simple and efficient approach. This strategy involved the synthesis and self-assembly of fluorinated raspberry-like particles. When solutions of these particles were cast onto glass substrates and subsequently evaporated, the resultant surfaces exhibited superamphiphobic properties. The raspberry-like structures of these particles provided the coatings with dual-scale roughness and re-entrant sites, while the functionalization of these particles with the fluorinated copolymer P(GMA-*co*-FOEMA) provided a low surface tension.

4.4 Future Work

This thesis described the preparation of raspberry-like particles that exhibited excellent superamphiphobic properties. These raspberry-like particles each consisted of a large central particle with a TEM diameter of 337 nm that were surrounded by numerous small particles that were 120 nm in diameter. The combination of these components thus provided the resultant coatings with a dual-scale roughness. Nevertheless, the optimization of this dual-scale surface roughness, particularly the sizes of the small and large particles, may help to further improve superamphiphobicity of the resultant coatings. In addition, the ring opening reaction between the epoxy-functionalized particles and amino-functionalized particles has been shown to proceed very rapidly. Thus, the efficiency of this covalent linkage reaction between the small and large particles will be investigated in attempts to shorten the reaction time while maintaining the effectiveness of the reaction. Furthermore, the influence of the amount of particles that are used to coat a substrate on the final performance of that surface will be also investigated. In addition, the degree of fluorination may provide another area where further optimization is possible. Due

to the cost of fluorinated materials, optimization may help to determine the ideal amount of the copolymer that can be used to provide the desired performance while avoiding waste of the copolymer.

Janus particles, named after the two faced Roman god, consist of two domains that possess different physical or chemical properties.[9] The coexistence of these two different regions within a single nanoparticle provides Janus particles with very unique properties. They have been widely investigated for their applications in electronics, textiles, sensors, magnetic field imaging, as well as for the stabilization of emulsions.[9-14]

In recent years, more effort has been devoted toward the development of different strategies for synthesizing Janus particles. Lattuada and Hatton have classified these synthetic techniques into three main categories that include masking, self-assembly, and phase separation.[15] The masking technique is the most flexible technique, which initially involves the protection of one side of a particle, which is followed by the modification of the unprotected side, and a subsequent deprotection step.[17] Meanwhile, the self-assembly technique utilizes changes to the solvent to induce the self-assembly of well-defined block polymers, and subsequently crosslinking treatment to lock the resultant structure.[16] Alternatively, the phase separation technique involves the mixing of two or more incompatible substances that then separate into their own domains that comprise distinct regions within a single nanoparticle.[18]

While raspberry-like particles can be produced under conditions when large particles are fed into a large excess of the small particles, Janus particles should be produced if the particles are fed in a 1:1 number ratio. Unfortunately, these conditions did not yield the desired structures, presumably due to the subsequent uncontrolled fusion of these Janus particles into large aggregates. We imagined that this situation could be avoided if the dimerization occurred more rapidly than the fusion process, and if the latter process could be prevented. This possibility

prompted us to re-examine the fusion of these particles and to propose an alternative strategy. Figure 4-1 illustrates this proposed procedure to synthesize the targeted Janus particles. Epoxy-functionalized particles would be quickly mixed with amino-functionalized particles of the similar size under vigorous stirring at room temperature. After a short period of time, an excess of hexylamine would be added to the mixture in order to terminate further reactions between the particles. Subsequent centrifugation of these products would yield Janus particle-enriched samples.

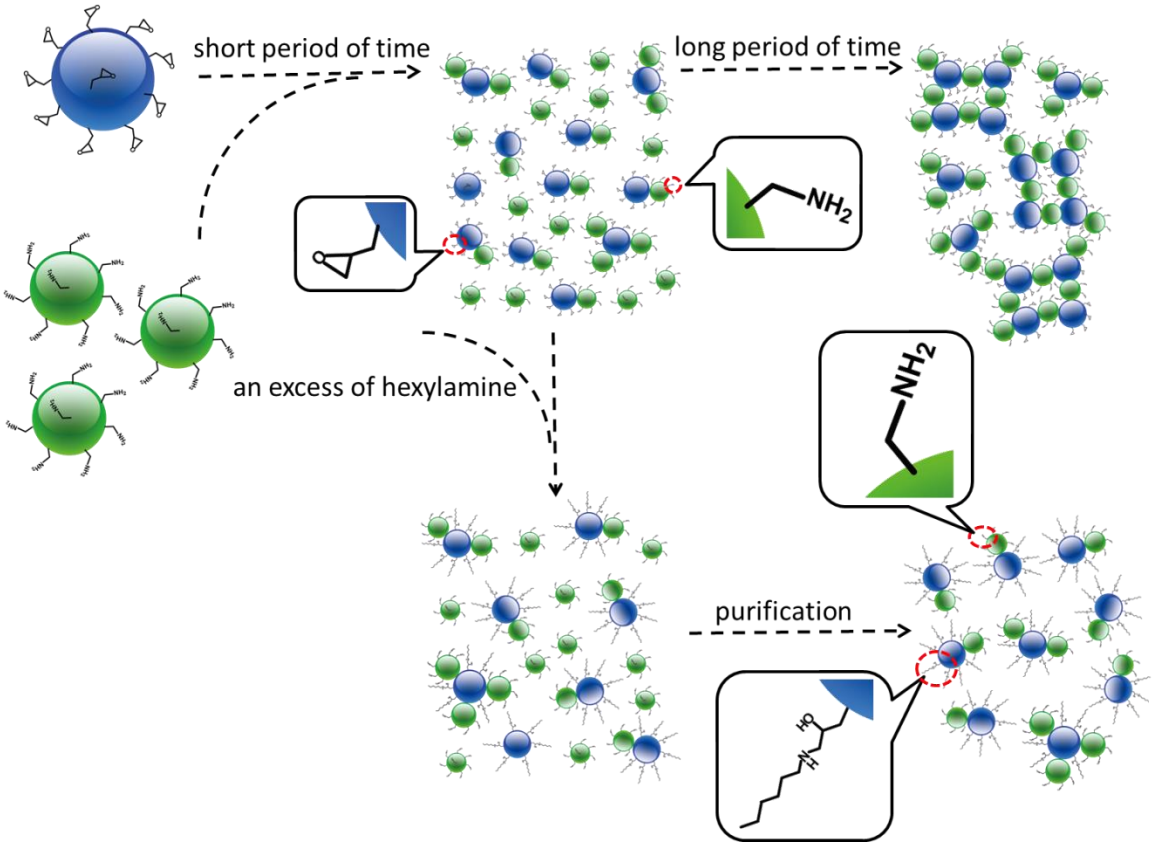

Figure 4-1 Schematic illustration of the proposed procedure for generating Janus particles.

In summary, raspberry-like particles were prepared and subsequently employed to prepare superamphiphobic coatings. While these raspberry-like particles provided highly effectively superamphiphobic coatings, further optimization of their preparation protocols may enhance their self-cleaning performance even further. In addition, the strategy utilized to prepare these raspberry-like particles through the fusion of precursor particles bearing amino and epoxy groups, may also open doors toward the preparation of Janus particles. These Janus particles composed of similar-sized constituent particles, may also provide effective ingredients for self-cleaning coatings, and may have potential for various other applications.

References

1. Bhushan, B.; Jung, Y. C. *Prog. Mater. Sci.* **2011,** *56*, 1-108.
2. Liu, K.; Tian, Y.; Jiang, L. *Prog. Mater. Sci.* **2013,** *58*, 503-564.
3. Tuteja, A.; Choi, W.; Ma, M.; Mabry, J. M.; Mazzella, S. A.; Rutledge, G. C.; McKinley, G. H.; Cohen, R. E. *Science*, **2007**, *318*, 1618-1622
4. Tuteja, A.; Choi, W.; Mabry, J. M.; McKinley, G. H.; Cohen, R. E. *Proc. Natl. Acad. Sci. USA*, **2008**, *105*, 18200-18205.
5. Zhao, H.; Law, K.Y.; Sambhy, V. *Langmuir*, **2011**, *27*, 5927-5935.
6. Zhao, H.; Park, K.C.; Law, K.Y. *Langmuir*, **2012**, *28*, 14925-14934.
7. Herminghaus, S. *Europhys. Lett.* **2000,** *52*, 165-170.
8. Deng, X.; Mammen, L.; Butt, H.-J.; Vollmer, D. *Science* **2012,** *335*, 67-70.
9. Li, F.; Josephson, D. P.; Stein, A., *Angew. Chem. Int. Ed.* **2011,** *50*, 360-388.
10. Nisisako, T.; Torii, T.; Takahashi, T.; Takizawa, Y., *Adv. Mater.* **2006,** *18*, 1152-1156.
11. Synytska, A.; Khanum, R.; Ionov, L.; Cherif, C.; Bellmann, C., *ACS Appl. Mater. Interfaces* **2011,** *3*, 1216-1220.
12. Yoshida, M.; Roh, K.-H.; Mandal, S.; Bhaskar, S.; Lim, D.; Nandivada, H.; Deng, X.; Lahann, J., *Adv. Mater.* **2009,** *21*, 4920-4925.
13. Hu, S.-H.; Gao, X., *J. Am. Chem. Soc.* **2010,** *132*, 7234-7237.
14. Walther, A.; Matussek, K.; Muller, A. H. E., *ACS Nano* **2008,** *2*, 1167-1178.
15. Lattuada, M.; Hatton, T. A., *Nano Today* **2011,** *6*, 286-308.
16. Nelson P.H., Rutledge G.C., Hatton T.A., *Comput. Theor. Polym. Sci.* **1988**, *8*, 31-38.
17. Takei H., Shimizu N., *Langmuir* **1997**, *13*, 1865-1868.
18. Carbone L., Cozzoli P.D., *Nano Today* **2010**, *5*, 449-493.